⌘ *Author's Choice*

THE JOURNAL OF BIOLOGICAL CHEMISTRY VOL. 289, NO. 41, pp. 28054–28069, October 10, 2014
© 2014 by The American Society for Biochemistry and Molecular Biology, Inc. Published in the U.S.A.

Structural and Mechanistic Insight into the *Listeria monocytogenes* Two-enzyme Lipoteichoic Acid Synthesis System*[S]

Received for publication, June 23, 2014, and in revised form, August 12, 2014 Published, JBC Papers in Press, August 15, 2014, DOI 10.1074/jbc.M114.590570

Ivan Campeotto[‡], Matthew G. Percy[‡], James T. MacDonald[§], Andreas Förster[§], Paul S. Freemont[§1], and Angelika Gründling[‡2]

From the [‡]Section of Microbiology and MRC Centre for Molecular Bacteriology and Infection, and the [§]Centre for Structural Biology, Imperial College London, London SW7 2AZ, United Kingdom

Background: *Listeria monocytogenes* lipoteichoic acid is synthesized by the LtaP/LtaS two-enzyme system.
Results: Structural analysis reveals a second glycerolphosphate binding site in LtaS important for *in vitro* and *in vivo* enzyme function.
Conclusion: These results suggest a binding mode for the lipoteichoic acid chain during polymerization.
Significance: The identified binding site in LtaS could become a target for antibiotic development.

Lipoteichoic acid (LTA) is an important cell wall component required for proper cell growth in many Gram-positive bacteria. In *Listeria monocytogenes*, two enzymes are required for the synthesis of this polyglycerolphosphate polymer. The LTA primase $LtaP_{Lm}$ initiates LTA synthesis by transferring the first glycerolphosphate (GroP) subunit onto the glycolipid anchor and the LTA synthase $LtaS_{Lm}$ extends the polymer by the repeated addition of GroP subunits to the tip of the growing chain. Here, we present the crystal structures of the enzymatic domains of $LtaP_{Lm}$ and $LtaS_{Lm}$. Although the enzymes share the same fold, substantial differences in the cavity of the catalytic site and surface charge distribution contribute to enzyme specialization. The $eLtaS_{Lm}$ structure was also determined in complex with GroP revealing a second GroP binding site. Mutational analysis confirmed an essential function for this binding site and allowed us to propose a model for the binding of the growing chain.

Lipoteichoic acid (LTA)[3] is an important cell wall component found in many Gram-positive bacteria, including human pathogens such as *Staphylococcus aureus* and *Listeria monocytogenes*. In its absence, bacteria are impaired in growth and show cell morphology and cell division defects (1–3). Therefore, enzymes involved in its synthesis are attractive targets for the design of new antimicrobials. This has been experimentally validated with the identification of a small molecule LTA synthesis inhibitor that prevented the growth of antibiotic-resistant Gram-positive bacteria as well as prolonging the survival of mice challenged with a lethal dose of *S. aureus* (4).

A common type of LTA consists of a linear 1,3-linked polyglycerolphosphate (PGP) polymer that is attached to the outside of the membrane via a glycolipid anchor (5, 6). In *L. monocytogenes*, the glycolipids anchor is Gal(α1–2)-Glc(α1–3)-diacylglycerol (Gal-Glc-DAG) or Gal(α1–2)Ptd-6-Glc(α1–3)-DAG (Gal-Ptd-6Glc-DAG), in which the glucose moiety is lipidated with an additional phosphatidyl (Ptd) group (5, 7, 8). The PGP backbone chain is polymerized by lipoteichoic acid synthase or LtaS-type enzymes (1). This class of enzyme uses the membrane lipid phosphatidylglycerolphosphate (PG) as a substrate, hydrolyzes the glycerolphosphate (GroP) head group of this lipid and subsequently adds it to the tip of the growing chain (9, 10). In *S. aureus* only one enzyme, namely $LtaS_{Sa}$, is required for LTA backbone synthesis. This enzyme initiates LTA synthesis by the transfer of the first GroP subunit onto the glycolipid anchor and subsequently polymerizes the backbone chain by the repeated addition of GroP subunits (1, 11). In contrast, *L. monocytogenes* uses a two-enzyme system for LTA synthesis (3). The lipoteichoic acid primase $LtaP_{Lm}$ transfers the initial GroP subunits to the glycolipid anchor but is unable to extend the chain further. Chain polymerization is performed by the lipoteichoic acid synthase $LtaS_{Lm}$ (3).

Regardless of whether LTA synthase or primase, LtaS-type enzymes, have the same overall architecture. They are composed of an N-terminal domain with five transmembrane helices, which is followed by an extracellular C-terminal domain (eLtaS) containing the catalytic site (recently reviewed in Ref. 12). For many organisms, including the human pathogens *S. aureus, Staphylococcus epidermidis*, *L. monocytogenes*, and *Bacillus anthracis*, it has been shown that LtaS is cleaved by an endogenous peptidase and a fraction of the extracellular eLtaS is released into the culture supernatant as well as partially retained within the cell wall fraction (3, 13–16). *In vitro*, the

* This work was supported by European Research Council Grant 260371 (to A. G.).
⌘ *Author's Choice*—Final version full access.
[S] This article contains supplemental Table S1.
[1] To whom correspondence may be addressed: Dept. of Medicine, Imperial College London, South Kensington Campus, Sir Ernst Chain Building, London SW7 2AZ, United Kingdom. Tel.: +44-207-594-5327; E-mail: p.freemont@imperial.ac.uk.
[2] To whom correspondence may be addressed: Section of Microbiology, South Kensington Campus, Flowers Building, Rm. 3.21, London SW7 2AZ, United Kingdom. Tel.: +44-207-594-5256; E-mail: a.grundling@imperial.ac.uk.
[3] The abbreviations used are: LTA, lipoteichoic acid; PGP, polyphosphatidylglycerol phosphate; DAG, diacylglycerol; PG, phosphatidylglycerolphosphate; Ptd, phosphatidyl; GroP, glycerolphosphate; PDB, Protein Data Bank; NBD, 7-nitrobenz-2-oxa-1,3-diazole-4-yl.

TABLE 1

Bacterial strains used in this study

Antibiotics were used at the following concentrations: for *E. coli* cultures: Ampicillin (AmpR) 100 μg/ml; kanamycin (KanR), 30 μg/ml; tetracycline (TetR), 10 μg/ml; for *L. monocytogenes* cultures: chloramphenicol (CamR), 7.5 μg/ml; streptomycin, 200 μg/ml (StrepR) for conjugation experiments.

Strain	Relevant features	Reference
***Escherichia coli* strains**		
XL1 Blue	Cloning strain, TetR – ANG127	Stratagene
SM10	*E. coli* strain used for conjugations; KanR – ANG618	40
DH-E898	XL1 Blue pPL3; *L. monocytogenes* integration vector; CamR – ANG1276	41
ANG1401	XL1 Blue pPL3-*lmo0927His6*; Lmo0927 ($LtaS_{Lm}$) with C-terminal His-tag under native promoter control; CamR	3
ANG1449	DH5α pProEX-$eLtaS_{Lm}$; plasmid for expression of $eLtaS_{Lm}$; AmpR	11
ANG1478	Rosetta pProEX-$eLtaP_{Lm}$; strain for overexpression of $eLtaP_{Lm}$; AmpR	11
ANG1479	Rosetta pProEX-$eLtaS_{Lm}$; strain for overexpression of $eLtaS_{Lm}$; AmpR	11
ANG2930	XL1-Blue pPL3-*lmo0927His6*-T307A; Lmo0927-T307A with C-terminal His-tag under native promoter control; CamR	This study
ANG2931	XL1-Blue pPL3-*lmo0927His6*-S486A; Lmo0927-S486A with C-terminal His-tag under native promoter control; CamR	This study
ANG2932	XL1-Blue pPL3-*lmo0927His6*-N488A; Lmo0927-N488A with C-terminal His-tag under native promoter control; CamR	This study
ANG2933	XL1-Blue pPL3-*lmo0927His6*-H489A; Lmo0927-H489A with C-terminal His-tag under native promoter control; CamR	This study
ANG2934	XL1-Blue pPL3-*lmo0927His6*-AAA; Lmo0927-AAA with C-terminal His-tag under native promoter control; CamR	This study
ANG2935	XL1-Blue pProEX-$eLtaS_{Lm}$-T307A; plasmid for expression of $eLtaS_{Lm}$-T307A variant; AmpR	This study
ANG2936	XL1-Blue pProEX-$eLtaS_{Lm}$-S486A; plasmid for expression of $eLtaS_{Lm}$-S486A variant; AmpR	This study
ANG2937	XL1-Blue pProEX-$eLtaS_{Lm}$-N488A; plasmid for expression of $eLtaS_{Lm}$-N488A variant; AmpR	This study
ANG2938	XL1-Blue pProEX-$eLtaS_{Lm}$-H489A; plasmid for expression of $eLtaS_{Lm}$-H489A variant; AmpR	This study
ANG2939	XL1-Blue pProEX-$eLtaS_{Lm}$-AAA; plasmid for expression of $eLtaS_{Lm}$-AAA variant; AmpR	This study
ANG2940	Rosetta pProEX-$eLtaS_{Lm}$-T307A; strain for overexpression of $eLtaS_{Lm}$-T307A variant; AmpR	This study
ANG2941	Rosetta pProEX-$eLtaS_{Lm}$-S486A; strain for overexpression of $eLtaS_{Lm}$-S486A variant; AmpR	This study
ANG2942	Rosetta pProEX-$eLtaS_{Lm}$-N488A; strain for overexpression of $eLtaS_{Lm}$-N488A variant; AmpR	This study
ANG2943	Rosetta pProEX-$eLtaS_{Lm}$-H489A; strain for overexpression of $eLtaS_{Lm}$-H489A variant; AmpR	This study
ANG2944	Rosetta pProEX-$eLtaS_{Lm}$-AAA; strain for overexpression of $eLtaS_{Lm}$-AAA variant; AmpR	This study
ANG1460	SM10 pPL3-*lmo0927His6*; KanR, CamR	This study
ANG2946	SM10 pPL3-*lmo0927His6*-T307A; KanR, CamR	This study
ANG2947	SM10 pPL3-*lmo0927His6*-S486A; KanR, CamR	This study
ANG2948	SM10 pPL3-*lmo0927His6*-N488A; KanR, CamR	This study
ANG2949	SM10 pPL3-*lmo0927His6*-H489A; KanR, CamR	This study
ANG2950	SM10 pPL3-*lmo0927His6*-AAA; KanR, CamR	This study
***Listeria monocytogenes* strains**		
10403S	StrepR – ANG1263	42
ANG1386	10403SΔ*lmo0927*; StrepR	This study
ANG1411	10403SΔ*lmo0927* pPL3; StrepR, CamR	This study
ANG1454	10403SΔ*lmo0927* pPL3-*lmo0927His6*; StrepR, CamR	This study
ANG2951	10403SΔ*lmo0927* pPL3-*lmo0927His6*-T307A; StrepR, CamR	This study
ANG2952	10403SΔ*lmo0927* pPL3-*lmo0927His6*-S486A; StrepR, CamR	This study
ANG2953	10403SΔ*lmo0927* pPL3-*lmo0927His6*-N488A; StrepR, CamR	This study
ANG2954	10403SΔ*lmo0927* pPL3-*lmo0927His6*-H489A; StrepR, CamR	This study
ANG2955	10403SΔ*lmo0927* pPL3-*lmo0927His6*-AAA; StrepR, CamR	This study

extracellular eLtaS has been shown to be sufficient for PG hydrolysis (11, 17). However, expression of the extracellular enzymatic domain is not sufficient for LTA production *in vivo* and the full-length membrane embedded LtaS protein is required for polymer production (16).

The structures of the extracellular enzymatic eLtaS domains of the *S. aureus* (PDB code 2W5Q) and *B. subtilis* (PDB code 2W8D) have been reported (13, 18). These previous studies showed that the enzymes are related to arylsulfatase family enzymes with the same α/β-barrel fold. A conserved metal binding site was revealed and its requirement for enzyme function confirmed experimentally (13). In addition, a Thr amino acid within the active center was identified as the catalytic residue and its essential role was confirmed as an $LtaS_{Sa}$-T300A variant was enzymatically inactive both *in vitro* and *in vivo* (13). The active site Thr was found to be phosphorylated in the *B. subtilis* and unmodified in the *S. aureus* structure, but the biological significance of this modification has not yet been determined. It was further hypothesized that the reaction proceeds through a covalent GroP-enzyme intermediate through the catalytic Thr (13).

To understand better the reaction mechanism and enzyme specificity of this class of proteins, we performed a structural analysis of the extracellular soluble domains of the two *L. monocytogenes* enzymes $eLtaP_{Lm}$ and $eLtaS_{Lm}$. This analysis revealed a substantially smaller cavity around the catalytic center in the primase enzyme compared with the synthase enzyme. The $eLtaS_{Lm}$ structure was also determined in complex with GroP. This led to the identification of a second GroP binding site in $eLtaS_{Lm}$ that is essential for enzyme function. Detailed bioinformatics analyses revealed specific motifs that differentiate LtaS and LtaP enzymes and highlighted that primase-related enzymes are only present in a small subset of bacteria. Taken together the structural and functional data allowed us to propose a revised mechanism for LTA biosynthesis in Gram-positive bacteria.

EXPERIMENTAL PROCEDURES

Plasmid and Strain Construction—Strains and primers used in this study are listed in Tables 1 and 2, respectively. *Escherichia coli* strains were grown in LB medium and *L. monocytogenes* strains in BHI medium. The cultures were grown at the

TABLE 2
Primers used in this study
Restriction sites are underlined.

Number	Name	Sequence
ANG674	5-PstI-Lmo0927-withP	AACTGCAGCTAGCAGACTTCCATTCCAAATGGTTC
ANG676	3-SalI-Lmo0927-C-His	ACGCGTCGACTTAGTGATGGTGATGGTGATGaccTTTATCGGATGAATCAGTTGATTTTTTC
ANG1649	5-Lmo0927-T307A	CCACCAAACTGGACAAGGGAAAGCAGCTGACTCCGAAATGTTAC
ANG1650	3-Lmo0927-T307A	GTAACATTTCGGAGTCAGCTGCTTTCCCTTGTCCAGTTTGGTGG
ANG1651	5-Lmo0927-S486A	GTACGGTGACCATTATGGTATTGCCGACAACCATGAAGAAGCAATG
ANG1652	3-Lmo0927-S486A	CATTGCTTCTTCATGGTTGTCGGCAATACCATAATGGTCACCGTAC
ANG1653	5-Lmo0927-N488A	GACCATTATGGTATTTCCGACGCCCATGAAGAAGCAATGACAAAAATTC
ANG1654	3-Lmo0927-N488A	GAATTTTTGTCATTGCTTCTTCATGGGCGTCGGAAATACCATAATGGTC
ANG1655	5-Lmo0927-H489A	CCATTATGGTATTTCCGACAACGCTGAAGAAGCAATGACAAAAATTCTTG
ANG1656	3-Lmo0927-H489A	CAAGAATTTTTGTCATTGCTTCTTCAGCGTTGTCGGAAATACCATAATGG
ANG1657	5-Lmo0927-AAA	GTACGGTGACCATTATGGTATTGCCGACGCCGCTGAAGAAGCAATGACAAAAATTCTTG
ANG1658	3-Lmo0927-AAA	CAAGAATTTTTGTCATTGCTTCTTCAGCGGCGTCGGCAATACCATAATGGTCACCGTAC

indicated temperatures and the growth medium was supplemented with antibiotics as indicated in Table 1. Plasmids for the expression of eLtaS$_{Lm}$ variants with T307A, S486A, N488A, and H489A single amino acid substitutions and the triple mutant S486A/N488A/H489A (AAA variant) were constructed by QuikChange mutagenesis using plasmid pProEX-eLtaS$_{Lm}$ (strain ANG1449) as template and primer pairs ANG1649/ANG1650, ANG1651/ANG1652, ANG1653/ANG1654, ANG1655/ANG1656, and ANG1657/ANG1658. The resulting plasmids were initially transformed into *E. coli* strain XL1-Blue yielding strains ANG2935 to ANG2939 and subsequently transformed for protein expressing into the *E. coli* Rosetta strain yielding strains ANG2940 to ANG2944. Plasmid pPL3-*lmo0927His6* (Strain ANG1401) allows for the expression of full-length LtaS$_{Lm}$ with a C-terminal His tag from its native promoter in *L. monocytogenes* (3). This vector was used as template for the construction of plasmids pPL3-*lmo0927His6*-T307A, pPL3-*lmo0927His6*-S286A, pPL3-*lmo0927His6*-N488A, pPL3-*lmo0927His6*-H489A, pPL3-*lmo0927His6*-AAA for the expression of the different LtaS$_{Lm}$ variants in *L. monocytogenes.* The desired mutations were introduced by SOE PCR. More specifically, plasmid pPL3-*lmo0927His6*-T307A was constructed by amplifying the front and back of *lmo0927* and introducing the desired point mutation using plasmid pPL3-*lmo0927His6* as template and primer pairs ANG674/ANG1650 and ANG676/ANG1649 in two separate PCR reactions. The two fragments were subsequently fused in a second round of PCR using primers ANG674/ANG676. The resulting product was digested with PstI and SalI and ligated with vector pPL3 that has been cut with the same enzymes. Plasmids pPL3-*lmo0927His6*-S286A, pPL3-*lmo0927His6*-N488A, pPL3-*lmo0927His6*-H489A, and pPL3-*lmo0927His6*-AAA were constructed using the same strategy and primers ANG1652 to ANG1658 as listed in Table 2. The resulting plasmids were initially recovered in *E. coli* strain XL1-Blue yielding strains ANG2930 to ANG2934 and subsequently transformed along with plasmid pPL3-*lmo0927His6* into *E. coli* strain SM10 yielding strains ANG1460 and ANG2946 to ANG2950. Next all plasmids were conjugated from SM10 into *L. monocytogenes* strain 10403SΔ*lmo0927* using a previously described method (19) but maintaining the *L. monocytogenes* 10403SΔ*lmo0927* strain at 30 °C throughout the procedure. This yielded *L. monocytogenes* strains ANG1454, and ANG2951 to ANG2955, which were also propagated at 30 °C. The sequences of all inserts were verified by automated fluorescence sequencing at the MRC Clinical Sciences Centre Genomics Core Laboratory, Imperial College London.

Protein Expression and Purification—Strains ANG1478 Rosetta pProEX-eLtaP$_{Lm}$ (11) and ANG1479 Rosetta pProEX-eLtaS$_{Lm}$ (11) were used for the expression and purification of N terminally His-tagged eLtaP$_{Lm}$ and eLtaS$_{Lm}$ proteins, respectively. Protein induction and nickel affinity purification were performed as previously described (11, 13). The proteins were further purified by size exclusion chromatography using a Superdex S200 16/60 column (GE Healthcare) and a 50 mM Tris-HCl, pH 7.5, 200 mM NaCl, 5% glycerol buffer system for eLtaS$_{Lm}$ and the different alanine substitution variants or 20 mM Tris-HCl, pH 7.5, for eLtaP$_{Lm}$. Protein-containing fractions spanning the main peak were pooled and concentrated to ~10 mg/ml using 10-kDa molecular mass cut-off Amicon filtration devices (Millipore), if not otherwise stated. These proteins were subsequently used in structural studies. eLtaS variants with T307A, S486A, N488A, and H489A single amino acid substitutions and a S486A/N488A/H489A (AAA variant) triple mutant were expressed in *E. coli* strains ANG2940 to ANG2944 (Table 1). *L. monocytogenes* strain 10403S pPL3-LtaS$_{Lm}$-His$_6$ (ANG1424) (3) was used for the expression and purification of eLtaS$_{Lm}$ from the native host.

Purification of Native eLtaS$_{Lm}$ from L. monocytogenes Culture Supernatant and Mass Spectrometry Analysis—The *L. monocytogenes* strain 10403S pPL3-LtaS$_{Lm}$-His$_6$ (ANG1424) (3), which contains a plasmid for the expression of the C terminally His-tagged LtaS$_{Lm}$ variant, was used for the purification of the secreted eLtaS$_{Lm}$ fragment directly from *Listeria* culture supernatant. This strain was grown overnight in 6 liters of BHI medium. The bacterial cells were pelleted by centrifugation for 10 min at 7,000 × *g* and the cleared culture supernatant was filtered and loaded into a nickel-nitrilotriacetic acid column for protein purification, as previously reported (16). The elution fractions containing the C terminally His-tagged eLtaS$_{Lm}$ protein were pooled together and concentrated to a final volume of ~50 μl at 0.5 mg/ml using a 10-kDa molecular mass cut-off Centricon. The sample was mixed with an equal volume of protein loading buffer and 5 μg of protein separated on a 12% SDS-PAGE gel alongside 100 μg of eLtaS$_{Lm}$ protein produced and purified from *E. coli* strain ANG1479. Protein bands were visualized by Coomassie staining. The eLtaS$_{Lm}$ protein bands were excised from the gel, digested with chymotrypsin, and subjected to mass spectrometry analysis at the TAPLIN Mass

spectrometry facility (Harvard Medical School, Boston, MA). The expected active site threonine containing peptide FHQTGQGKTADSEM (T catalytic threonine) has a calculated mass of 1536.6 Da when unmodified or 1616.6 Da with a phosphorylated threonine residue.

Protein Crystallization and Structure Determination—The solubility of eLtaP$_{Lm}$ was 120 mg/ml in 20 mM Tris-HCl, pH 7.5, buffer and most crystallization drops remained clear in the initial screens. To decrease the solubility, the protein was subjected to Lys-methylation (20). Crystals appeared after 7–10 days at 4 °C in 100 mM sodium cacodylate buffer, pH 5.4, 100 mM $MgCl_2$, 33% PEG2000 at a protein concentration of 40 mg/ml. Crystals were flash cooled in liquid nitrogen without additional cryoprotection. Non-methylated protein alone failed to produce crystals under these conditions. However, macro-seeding or micro-seeding using the methylated protein promoted crystallization of the non-methylated protein. Therefore a methylated seed stock, stored at stored at 4 °C, was routinely used for seeding. Data were collected at the SOLEIL synchrotron at the PROXIMA1 beamline (Saint-Aubin, France) from a single crystal at 100 K. The crystal belonged to space group P1 with unit cell parameters $a = 53.20$ Å, $b = 53.70$ Å, $c = 85.07$Å; $\alpha = 71.57°$, $\beta = 87.89°$, $\gamma = 65.12°$. A mini-κ goniometer was used to obtain high completeness in all resolution shells. Data were indexed with XDS (21) and reduced with SCALA (21, 22) to 1.75-Å resolution. The R_{free} set was generated randomly in UNIQUE (23). The structure was solved by molecular replacement using PHASER as implemented in PHENIX AutoMR (24) using, after side chain pruning and ligands removal in SCULPTOR (24), the *S. aureus* eLtaS structure as model (PDB 2W5Q). Initial refinement and model building were performed in PHENIX AutoBuild and completed by cycles of reiterated manual building in COOT (25) and refinement in REFMAC (26). Structure validation was performed using MOLPROBITY (27).

Crystals of eLtaS$_{Lm}$ grew in 5–7 days at 20 °C in 0.64 M sodium acetate, pH 4.6, 4% PEG3350, 100 mM $MgCl_2$ and were cryo-protected with 25% PEG400 before flash-cooling in liquid N_2. A micro-seeding technique was employed to improve the crystal size (28) and crystallization trials were repeated in the same buffer conditions but lowering the protein concentration to 5 mg/ml. For the GroP co-crystallization experiments, the protein was incubated for 10 min at room temperature with a final concentration of 50 mM GroP. The crystals obtained from the co-crystallization were further soaked for 5 min in crystallization buffer supplemented with 25% PEG400 and 50 mM GroP before flash cooling in liquid N_2. Data collection of the apo-eLtaS$_{Lm}$ was performed at the Diamond Light Source synchrotron, beamline I24 (Didcot, Oxford, UK), from a single crystal at 100 K. The apo-structure of eLtaS$_{Lm}$ belonged to the space group $P4_12_12$ with unit cell dimensions of $a = b = 119.76$ Å, $c = 473.91$ Å; $\alpha = \beta = \gamma = 90.0°$. The data were indexed, scaled, and R_{free} was generated randomly in UNIQUE (23). The structure was solved by molecular replacement using BALBES (29) and the *B. subtilis* eLtaS$_{Bs}$ structure (PDB code 2W8D) as a starting model. Rigid body and restrained refinement produced a drop of R_{factor} and R_{free} from 42 and 43% to 25 and 31%, respectively. The structure was refined and validated as described above for eLtaP$_{Lm}$.

The data collection of the eLtaS$_{Lm}$-GroP complex was performed at the Diamond Light Source synchrotron beamline I04-1 (Didcot, Oxford, UK) from a single crystal at 100 K. The crystals belonged to the space group $P2_12_12_1$ with unit cell dimensions of $a = 119.25$ Å, $b = 119.63$ Å, $c = 472.66$ Å; $\alpha = \beta = \gamma = 90.0°$. Indexing was performed in XDS and data merging was performed in SCALA and TRUNCATE (23) H- and L-test analysis in TRUNCATE highlighted the presence of pseudo-meroheydral twinning. The R_{free} set was generated randomly in UNIQUE and the structure was solved by molecular replacement in PHASER using apo-eLtaS$_{Lm}$ as a model. Ten cycles of rigid body refinement (10.0–6.0 Å) followed by 10 cycles of restrained refinement in REFMAC gave an R value of 23.6% and R_{free} of 25.0%. Twin refinement in REFMAC highlighted a twin fraction of 9% with twinning operator *k, h, -l*. Therefore the twin option was kept for the whole refinement process, which was iterated with manual building in COOT. The final step of the refinement with rotamer optimization was performed in PHENIX, which did not detect any twinning. Composite omit maps were calculated in PHENIX and used to orient the terminal OH group of GroP. Structure validation was performed using MOLPROBITY. Ligand coordinate and dictionary files were generated and regularized in JLIGAND (30). Anomalous maps were generated using the SFTOOLS (23) and visualized in PYMOL. The statistics for all data sets are shown in Table 3.

One-dimensional ^{1}H NMR Analysis of eLtaP$_{Lm}$—10 mg of eLtaP$_{Lm}$ in 1 ml of 20 mM Tris-HCl, pH 7.5 buffer, was used for the one-dimensional ^{1}H NMR analysis. 10% D_2O was added to the protein sample and the spectra were recorded at 800 MHz at 37 °C before and after the addition of 10 mM EDTA final concentration.

Modeling of the GroP Trimer in the Catalytic Site of eLtaS$_{Lm}$—The coordinate and restraint files of the GroP trimer in its energy minimized form were generated with JLIGAND (30). Superposition of the coordinates of the GroP trimer with the eLtaS-GroP complexes was performed in PYMOL.

Enzyme Activity Assay—The activity of wild-type eLtaS$_{Lm}$ and eLtaS$_{Lm}$ variants T307A, S486A, N488A, H489A, and S486A/N488A/H489A was determined as previously reported (11). Briefly, 4 μg of the fluorescently labeled NBD-PG lipid substrate was incubated for 3 h at 37 °C with 30 μg of enzyme in 10 mM sodium succinate buffer, pH 6.0, adjusted to an ionic strength of 50 with NaCl and 10 mM $MnCl_2$. The lipid reaction products were subsequently extracted with chloroform and methanol, separated by thin layer chromatography, and the signal of the NBD-DAG hydrolysis product quantified as previously described (11). Each TLC plate contained a negative no-enzyme control lane to determine the background signal, as well as a wild-type eLtaS$_{Lm}$ enzyme reaction, which was for normalization purposes set to 100%. The activity of the different variants was calculated as percentage of activity compared with the wild-type control reaction. Four independent experiments with two different protein purifications were performed and the average percentage of activity and standard deviation were plotted.

TABLE 3
Dataset statistics
The information for the last shell of resolution is given in parentheses.

	eLtaP apo	eLtaS apo	eLtaS-GroP
Synchrotron	Soleil	Diamond	Diamond
Beamline	Proxima1	I24	I04–1
Space group	P_1	$P4_12_12$	$P2_12_12_1$
a, *b*, *c* (Å)	53.20	119.76	119.25
α, β, γ (°)	53.70	119.76	119.63
	85.04	473.91	472.66
	71.63	90.00	90.00
	76.78	90.00	90.00
	65.12	90.00	90.00
Resolution (Å)	47.96 (1.84-1.75)	106.88 (3.16-3.00)	48.71 (2.32-2.20)
R_{merge} [a]	0.069 (0.501)	0.117 (0.560)	0.089 (0.459)
R_{pim} [b] (all I^+ and I)	0.040 (0.293)	0.062 (0.318)	0.052 (0.265)
$\langle I \rangle$/SD $\langle I \rangle$	10.7 (2.5)	8.6 (2.3)	11.5 (2.7)
Completeness (%)	94.8 (92.6)	90.7 (84.6)	98.2 (95.7)
Redundancy	3.8 (3.8)	4.0 (3.5)	3.8 (3.8)
No. reflections	293,738 (41,866)	257,649 (29941)	1,285,177 (180393)
No. unique	77,013 (11,049)	63,877 (8,525)	335,456 (47,358)
R_{factor} [c]	0.178 (0.296)	0.222 (0.319)	0.178 (0.208)
R_{free} [d]	0.207 (0.330)	0.260 (0.376)	0.214 (0.237)
No. atoms	7,119	16,745	40,238
Protein	6,604	16,740	37,131
Water	481		2,997
Ligands	34	5	110
Average B-factors (Å^2)	31.4	50.9	33.1
Protein	30.9	50.9	33.0 (30.6)[e]
Waters	37.0		33.7
Ligands	44.7	45.5	38.6
Root mean square deviations			
Bond lengths (Å)	0.009	0.006	0.007
Bond angles (°)	1.23	0.93	1.07
Ramachandran most favored (%)	97	97	98
Ramachandran additional allowed (%)	3	3	2
Ramachandran outliers (%)	0	0	0
PDB code	4UOP	4UOO	4UOR

[a] $R_{merge} = \Sigma_h\Sigma_l |I_{hl} - \langle I_h \rangle| / \Sigma_h\Sigma_l \langle I_h \rangle$, where I_{hl} is the *l*th observation of reflection h and $\langle I_h \rangle$.
[b] R_{pim} as described in Ref. 43.
[c] $R_{factor} = \Sigma_h ||F_{obs(h)}| - |F_{cal(h)}|| / \Sigma_h |F_{obs(h)}|$, where $F_{obs(H)} - F_{cal(h)}$ are the observed and calculated structure factors for reflection *h*, respectively.
[d] R_{free} factor was calculated same as R_{factor} using 5% reflections, which were selected randomly and omitted from refinement.
[e] B-factor calculated excluding the disordered monomer K.

LTA and Protein Detection by Western Blot—The different *L. monocytogenes* strains were grown overnight at 30 °C in BHI medium. Sample analysis for the detection of LTA or the His-tagged LtaS variants by Western blot was performed as previously described (3).

Listeria Growth Curves and Microscopy Analysis—The indicated *L.* monocytogenes strains were grown overnight at 30 °C in BHI medium. The next day, the cultures were back diluted to an A_{600} of 0.05, incubated at 37 °C with shaking, and growth was monitored by determining A_{600} readings at timed intervals. For microscopy analysis, the different *L. monocytogenes* strain was propagated for at least 6 h at 37 °C in BHI medium. Subsequently culture aliquots were adjusted to an A_{600} of 0.5 and analyzed by phase-contrast microscopy using a Nikon Eclipse TS100 microscope with a ×20 objective. Images were recorded using a Sony HDR-CX11 high-definition camcorder mounted onto the microscope. Two independent microscopy experiments and three independent growth curves were performed and representative results are shown.

Bioinformatics and Sequence Analysis—Sequences homologous to the full-length LtaS and LtaP sequences were retrieved from the RefSeq microbial non-redundant database (31) using PSI-BLAST (32) with an *E*-value cutoff 1e-40. Sequences were filtered to have an alignment length of at least 400 residues, an identity of at least 28.7%, and similarity of 48.5% to either LtaS or LtaP. These cutoff values were chosen as they are the sequence identity and similarity between LtaS and LtaP. Sequences with a higher similarity to LtaP than LtaS were assigned to a primase-like sequence list (50 sequences), whereas sequences with a higher similarity to LtaS were assigned to a synthase-like list (1038 sequences). The LtaP and LtaS sequences were separately aligned using MUSCLE (33) and then combined using MUSCLE profile-profile alignment. The phylogenetic tree using the combined alignment (having removed any columns not aligned to either LtaS or LtaP) was generated using the program PROML from PHYLIP version 2.3 (34) and plotted using the R package APE (35). All logo plots were produced using WebLogo (36). For the PSICOV (37) amino acid covariation analysis a new larger alignment was produced of $LtaS_{Lm}$ homologous retrieved from the non-redundant database using PSI-BLAST and an *E*-value cutoff of 10^{-10}. These sequences were individually aligned to the $LtasS_{Lm}$ sequence using the BLOSUM62 matrix and Smith-Waterman algorithm, insertions were removed and pairwise alignments were combined to produce a multiple sequence alignment. Redundant sequences and sequences covering less than 60% of the $LtaS_{Lm}$ sequence were removed resulting in 6943 final sequences. This final alignment was subsequently analyzed using the residue contact prediction program PSICOV (37).

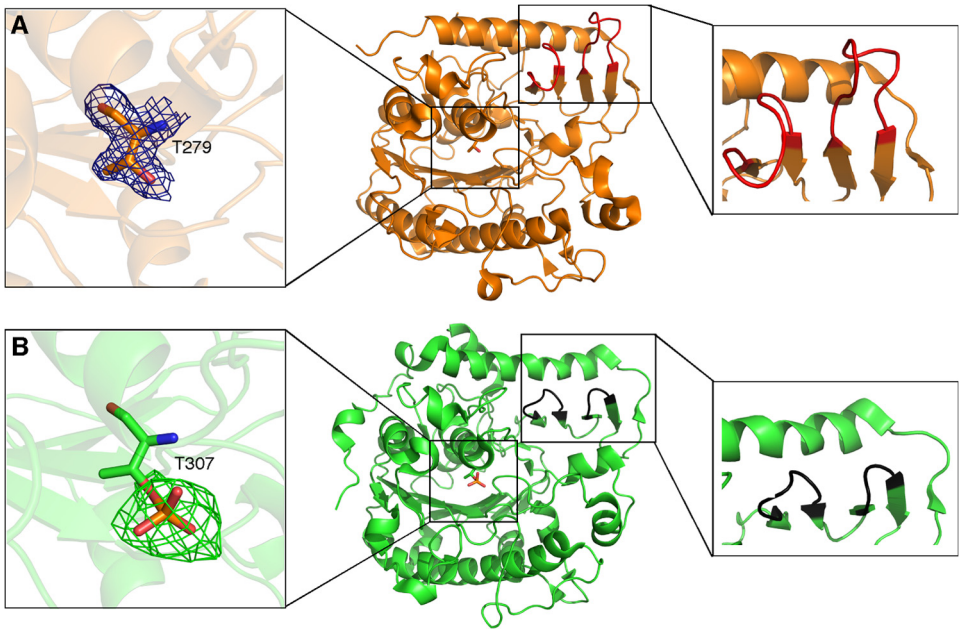

FIGURE 1. **Crystal structures of apo-eLtaP$_{Lm}$ and apo-eLtaS$_{Lm}$.** Schematic representation of the crystal structures of eLtaP$_{Lm}$ (*A*) and eLtaS$_{Lm}$ (*B*) with close ups of the catalytic Thr residues (*left panel*) and loop regions (*right panel*). The structural differences in the loop regions between eLtaP$_{Lm}$ and eLtaS$_{Lm}$ are highlighted in *red* and *black*, respectively. The $2F_o - F_c$ electron density map (1.0 root mean square deviation) of Thr-279 in eLtaP$_{Lm}$ is highlighted in *blue* and the omit $F_o - F_c$ map (3.0 root mean square deviation) of the phospho-Thr-307 in eLtaS$_{Lm}$ is highlighted in *green*.

RESULTS

Apo-structures of eLtaP$_{Lm}$ and LtaS$_{Lm}$—To identify differences between LTA synthase and primase enzymes, the soluble extracellular enzymatic domains eLtaP$_{Lm}$ and eLtaS$_{Lm}$ were overexpressed and purified from *E. coli* and their crystal structures were determined at 1.75- and 3.0-Å resolution, respectively. Although both enzymes were monomers in solution, as assessed by size exclusion chromatography, eLtaP$_{Lm}$ crystallized with two molecules in the asymmetric unit and eLtaS$_{Lm}$ with five molecules in the asymmetric unit (Table 3). The overall structures of eLtaS$_{Lm}$ and eLtaP$_{Lm}$ are very similar (root mean square deviation = 1.4 Å for Cα atoms). Both comprise an α/β core and a C-terminal part of four anti-parallel β-strands and a long α-helix (Fig. 1). As predicted, both enzymes are similar to eLtaS$_{Sa}$ (PDB code 2W5Q) and eLtaS$_{Bs}$ (PDB code 2W8D) with a root mean square deviation on Cα atoms of 1.7 Å for eLtaP$_{Lm}$ and 0.9 Å for eLtaS$_{Lm}$. Although the electrostatic surface potentials of eLtaS$_{Lm}$ and eLtaP$_{Lm}$ are similar around the α/β core at the N-terminal end, there are substantial differences in cavity size and surface charge distribution around the catalytic centers (Fig. 2, *A* and *B*).

A structure/sequence comparison of the two enzymes highlighted two sequence insertions in LtaP that form two extended loops (residues 544–552, loop 1; residues 561–570, loop 2), which interact with the long helix α18 (Figs. 1 and 2). There is no sequence conservation in loop 1 and loop 2 between eLtaP$_{Lm}$ and eLtaS$_{Lm}$ except for the salt bridge formed by residues Asp-600 and Arg-545, which correspond to Asp-616 and Arg-576 in the synthase enzyme. The insertion loop 2 in eLtaP$_{Lm}$ forms a negatively charged protrusion, which is repositioned through Phe-566 on α18 by ~2 Å compared with eLtaS$_{Lm}$. This also leads to the formation of a surface groove, which extends to the catalytic site (Fig. 2*C*). In eLtaS$_{Lm}$, this surface groove is constricted by Lys-306, which form a hydrogen bond with Tyr-483 (Fig. 2*D*). The specific loop 1 and loop 2 sequence insertions are conserved within primase homologues (Fig. 2, *E* and *F*) suggesting that the resulting surface features are specific for the function of primase enzymes.

The Catalytic Threonine Is Unmodified in the Natural Host—The catalytic residue of LtaS-type enzymes is a highly conserved Thr residue that in the *B. subtilis* eLtaS$_{Bs}$ structure is phosphorylated but unmodified in the *S. aureus* eLtaS$_{Sa}$ structure (13, 18). In this study, we found that Thr-307 in eLtaS$_{Lm}$ is phosphorylated, whereas the corresponding residue Thr-279 in eLtaP$_{Lm}$ is unmodified (Fig. 1). To gain insight into the physiological relevance of this modification, a C terminally His-tagged LtaS$_{Lm}$ variant was expressed in *L. monocytogenes* and the cleaved eLtaS$_{Lm}$ domain was purified from the culture supernatant. The purified protein was digested with chymotrypsin, and peptide fragments were analyzed by electron spray mass spectrometry. This analysis showed that for eLtaS$_{Lm}$ expressed in *E. coli* the catalytic Thr is mostly phosphorylated (73%), whereas only 2% of the protein purified from the natural host is phosphorylated (Fig. 3). These data suggest that phosphorylation of the catalytic Thr is not physiological but is likely a result of expression in a heterologous host. However, as shown below this modification is likely a mimic of an enzyme-substrate intermediate.

Preferential Binding of Mn^{2+} to the Conserved Metal Binding Site—LtaS-type proteins are metal-dependent enzymes and the highest *in vitro* enzyme activity is observed in the presence of Mn^{2+} (11, 17). Our data show that the metal binding site is identical in the LtaS$_{Lm}$ and LtaP$_{Lm}$ structures. In previous LtaS crystal structures both Mn^{2+} and Mg^{2+} were identified in the metal binding site near the catalytic threonine, facilitating phosphatidylglycerol hydrolysis (13, 18). As the crystallization

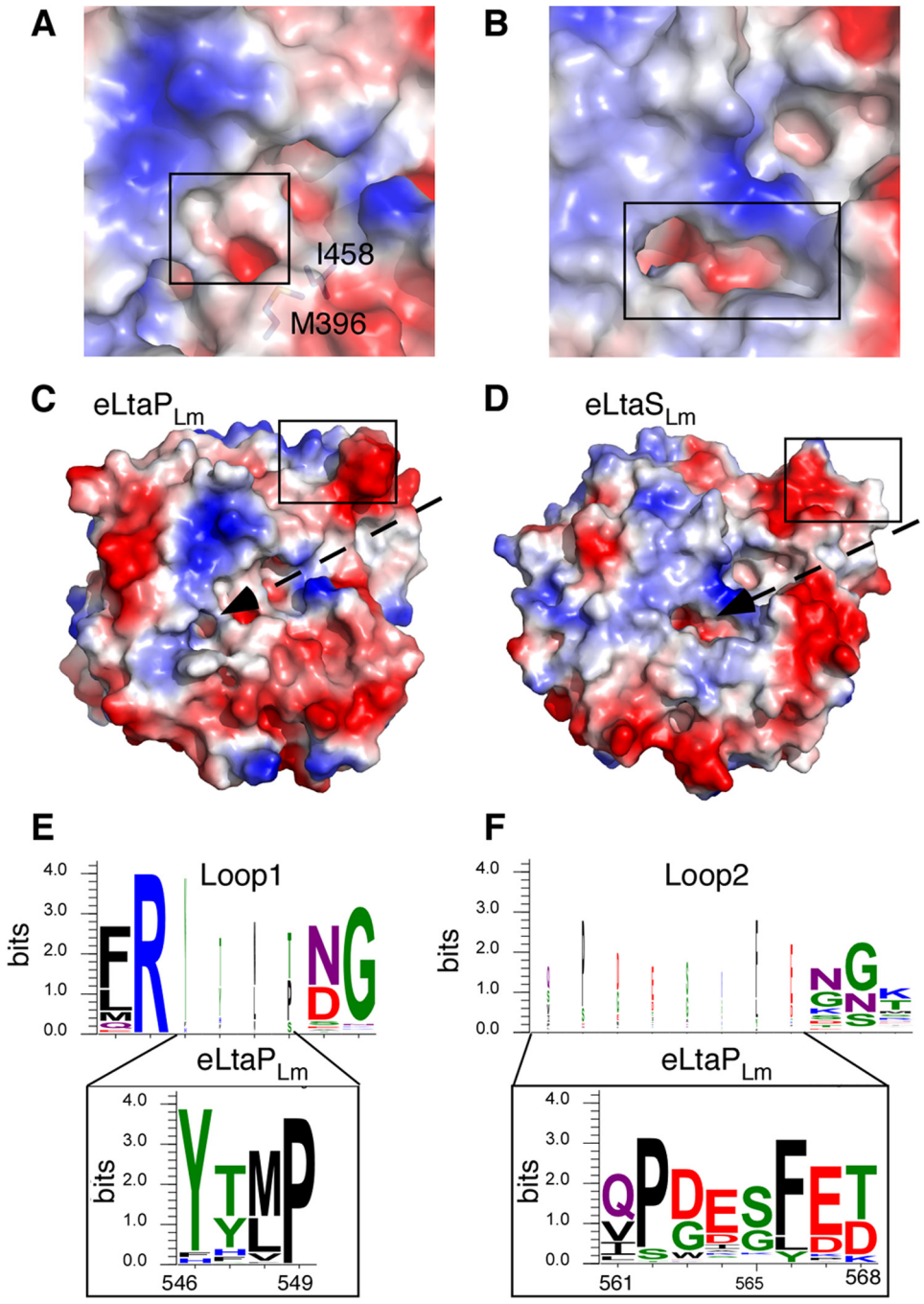

FIGURE 2. *A* and *B*, comparison of the catalytic pocket of eLtaP$_{Lm}$ and eLtaS$_{Lm}$. Surface potential representation (*blue*, positive; *red*, negative; *white*, hydrophobic) of the area around the catalytic site of eLtaP$_{Lm}$ (*A*) and eLtaS$_{Lm}$ (*B*). The catalytic pocket of eLtaP$_{Lm}$ is restricted through the highlighted amino acids Met-396 and Ile-458 and therefore significantly smaller and more hydrophobic than in eLtaS$_{Lm}$. *C* and *D*, surface potential representation of eLtaP$_{Lm}$ (*C*) and eLtaS$_{Lm}$ (*D*) structures with insertion loop regions *boxed* and a hydrophobic groove (*white*) stretching from loop 2 to the active site in eLtaP$_{Lm}$ as indicated. *E* and *F*, web logo motif for the insertion loop 1 (*E*) and insertion loop 2 (*F*) region of the top 1090 LtaS-type sequences shown on *top* and the web logo motif for the 51 LtaP-type sequences shown *below*, using amino acid numbering for LtaP$_{Lm}$. The dimension of the letters in WebLogos are directly proportional to the degree of conservation of the given residue.

buffer for both *Listeria* proteins contained a high $MgCl_2$ concentration, it is likely that Mg^{2+} is present in the active center in our structures. To determine the metal preference of the enzymes, crystallization trials were set up in the absence of any added metal ion. Although the eLtaP$_{Lm}$ protein did not crystallize under these conditions, one-dimensional ^1H NMR experiments showed an increase in peak sharpness upon addition of EDTA, suggesting the presence of a paramagnetic ion such as Mn^{2+} (Fig. 4*A*). Although the eLtaS$_{Lm}$ crystals grown in the absence of any added metal ion diffracted only to 6.4 Å, anomalous difference maps showed a strong anomalous peak consistent with the presence of a bound Mn^{2+} ion after expression and purification (Fig. 4*B*). Together our data provide evidence for preferential Mn^{2+} binding of both eLtaP$_{Lm}$ and eLtaS$_{Lm}$, in the

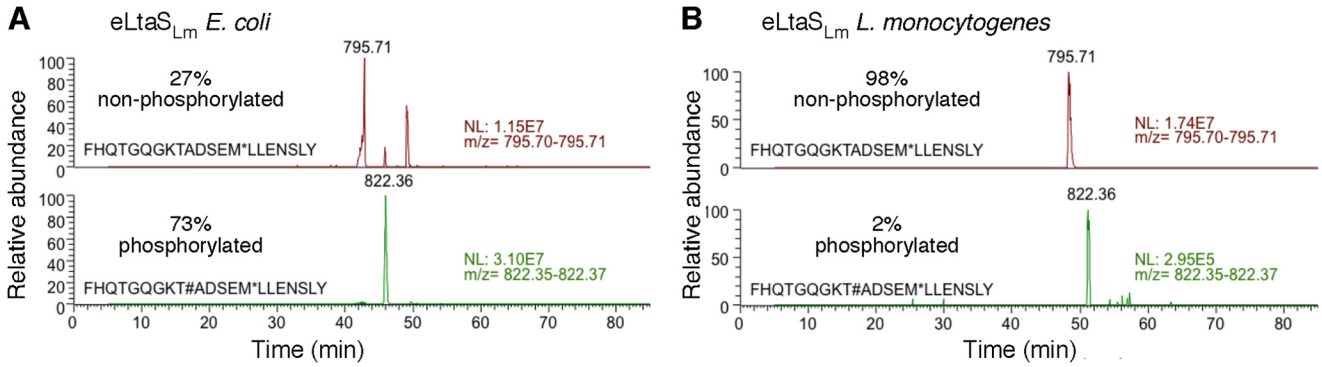

FIGURE 3. **Phosphorylation state of active site Thr as determined by mass spectrometry.** *A,* eLtaS$_{Lm}$ was purified from the *E. coli* cytoplasm or *B,* directly from the supernatant of a *L. monocytogenes* culture, separated on an SDS-PAGE gel, and subjected to a chymotrypsin digest and mass spectrometry analysis. The mass spectrometry traces corresponding to the active site containing peptide are shown for eLtaS$_{Lm}$ purified from *E. coli* (*A*) or *L. monocytogenes* (*B*). The expected active site threonine containing peptide FHQTGQGKTADSEM (T, catalytic threonine) has a calculated mass of 1536.6 Da when unmodified or 1616.6 Da with a phosphorylated Thr residue. The fraction of protein with a phosphorylated active site Thr was estimated based on the intensity of the mass spectrometry signal and is indicated in % in each panel.

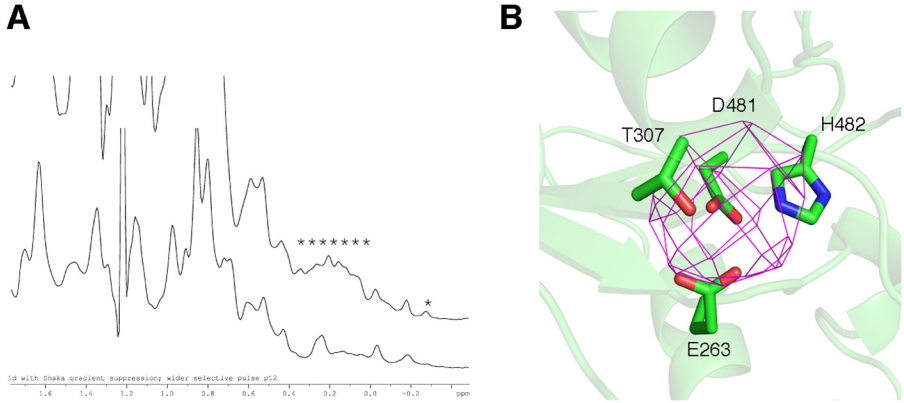

FIGURE 4. **Characteristics of enzyme-bound metal.** *A*, one-dimensional ^{1}H NMR spectra of eLtaP$_{Lm}$ in the absence or presence of EDTA one-dimensional NMR spectra of purified eLtaP$_{Lm}$ protein recorded on a 800 MHz magnet at 37 °C before and after addition of 10 mM EDTA. *B,* anomalous electron density map of eLtaS$_{Lm}$. eLtaS$_{Lm}$ crystals were grown in the absence of any added metal ions and data collected close to the Mn^{2+} edge (1.28 Å). The DANO SigDANO electron density map (shown in *purple*) confirms the presence of a Mn^{2+} ion.

absence of added metals consistent with previous biochemical activity measurements.

Identification of GroP Binding Sites in eLtaS$_{Lm}$—LtaS-type enzymes belong to the arylsulfatase group of enzymes and the reaction mechanism of other members of this class of enzymes proceeds through the formation of a covalent enzyme-substrate intermediate. In the case of sulfatases, a post-translationally modified cysteine residue, a hydroxyformylglycine, is sulfated during catalysis (38). We previously speculated that LtaS-type enzymes also form a covalent GroP-Thr intermediate as part of the reaction mechanism (13). Although we show here that the phosphorylation of the active site Thr residue observed in the eLtaS$_{Lm}$ structure does not occur in the native host (Fig. 3), its presence in *E. coli* could, however, mimic such a covalent enzyme substrate intermediate. To provide additional experimental evidence for the formation of a covalent GroP-Thr intermediate, we performed co-crystallization and crystal soaking experiments with the eLtaS$_{Lm}$ and PG lipid substrates with short chain fatty acids. However, co-crystallization experiments failed to produce crystals and crystal-soaking experiments abolished the diffraction power of the crystals. Next, co-crystallization and soaking experiments were performed with GroP, the hydrolysis product of the lipid substrate PG, and the structure was solved from crystals containing 11 molecules in the asymmetric unit.

Using this approach, extra electron density was observed in each monomer within the catalytic site (Fig. 5). Similar as in the apo-structure, it was possible to build a phosphate group into a density extending from Thr-307 (Fig. 5). The phosphate oxygen binds to two structurally conserved water molecules, Trp-360, His-422, and a Mg^{2+} ion that is in turn further coordinated by Glu-263, Asp-481, and His-482 (Fig. 6, *A* and *B*). Additional difference electron density was observed in each monomer at the entrance of the catalytic pocket, into which a GroP molecule could be built (Fig. 5). In all chains, the phosphate group of the GroP molecule in this second site formed hydrogen bonds with residues Ser-486, Asn-488, and His-489 (Fig. 6, *A* and *B*). In eight molecules in the asymmetric unit an additional hydrogen bond was observed between the terminal hydroxyl group of GroP and a water molecule (W1), which in turn forms a hydrogen bond with Tyr-483 (Fig. 6*B*). In a previous study, the co-crystal structure of the *S. aureus* active site variant eLtaS$_{Sa}$-T300A with a GroP molecule within the active center was determined (PDB code 2W5R) (13). The overlay of the catalytic sites of the GroP-eLtaS$_{Sa}$-T300A and the GroP-eLtaS$_{Lm}$ structures revealed that the GroP molecule within the active center

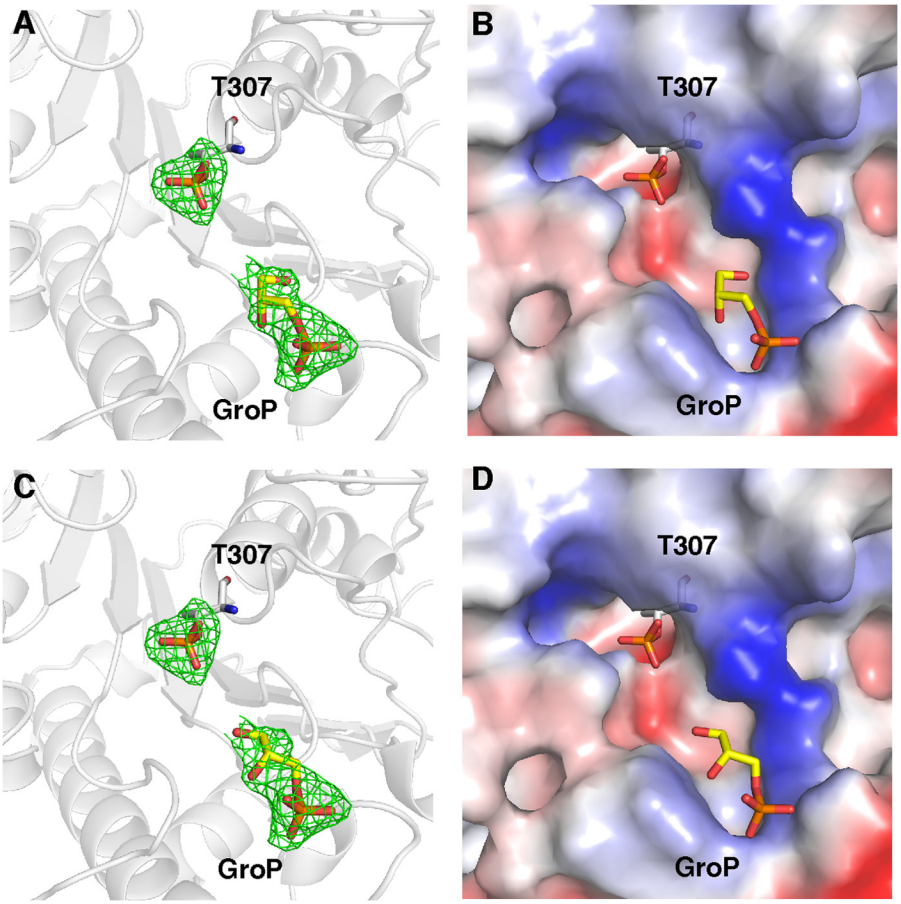

FIGURE 5. **GroP/eLtaS$_{Lm}$ co-crystal structure.** *A,* ribbon representation of the active site of eLtaS$_{Lm}$ with bound phosphate and a GroP molecule in a second site, as observed in chains B, C, D, F, H, I, J, and K. The phosphate group is covalently linked to the catalytic Thr-307 and GroP is bound at the entrance of the catalytic site. The omit $F_o - F_c$ electron density map (3.0 root mean square deviation) of the phospho-threonine (*T307*) and GroP are shown in *green*. *B*, electrostatic surface potential representation (*blue*, positive; *red*, negative) around the catalytic site showing the charge distribution surrounding the phospho-Thr-307 and the GroP molecule. *C,* ribbon representation of the active site of eLtaS$_{Lm}$ with bound phosphate and a GroP molecule in a second site (as observed in chains A, E, and G) and *D,* the corresponding surface potential representation.

(referred to as GroP1) superposed with the phosphothreonine and the conserved water molecules W2 and W3 in eLtaS$_{Lm}$ (Fig. 6*C*). Therefore, the phosphorylated Thr likely mimics a covalent GroP-Thr intermediate. The distance between the phosphorylated Thr and the terminal hydroxyl group of the GroP2 molecule bound at the entrance of the catalytic pocket is ~6.3 Å, which is compatible with the length of one intervening GroP molecule. To test whether an additional GroP molecule could fit into this space, a GroP trimer model was generated *in silico* and fitted into the eLtaS$_{Lm}$ structure using the experimental electron densities of the phosphothreonine and GroP as a guide (Fig. 6*D*). Our modeling showed that a GroP could fit in the intervening space suggesting that the growing PGP LTA chain could be bound in a similar manner during the catalytic cycle of eLtaS$_{Lm}$. The nature of the surface potential of the oligo-GroP binding groove further supports this conclusion (Fig. 6*E*). A series of ordered water molecules spans the catalytic site of eLtaS$_{Lm}$ from residue His-353 to the trapped GroP2 molecule. The positions of these water molecules are conserved across all 11 monomers within a crystallographic unit and trace the position of the modeled GroP trimer (Fig. 6).

The Second GroP Binding Site in eLtaS$_{Lm}$ Is Essential for Enzyme Function—To test the functional requirement of the second GroP binding site, we mutated residues Ser-486, Asn-488, and His-489 to alanines individually or in combination and tested the mutant enzymes for their ability to produce LTA (Fig. 7). The different variants were expressed as C-terminal His tag fusion proteins in the *L. monocytogenes* strain 10403SΔ*ltaS*, which contains a deletion of the native *ltaS* gene. As negative controls, an empty vector or a vector for the expression of the catalytic site variant T307A (pPL3-*ltaS*$_{T307A\text{-}His6}$) were introduced into 10403SΔ*ltaS* and as positive control a vector for expression of wild-type LtaS (pPL3-*ltaS*$_{His6}$). Expression of all LtaS variants was confirmed by Western blot. As previously reported for WT LtaS$_{Lm}$ (3), all GroP binding site variants were cleaved and the eLtaS fragment was detected in the culture supernatant as well as in the cell wall-associated fraction (Fig. 7*A*). The active site T307A variant remained unprocessed and the full-length protein was observed in the cell wall-associated fraction (Fig. 7*A*). In a previous study, a similar accumulation of the full-length protein was observed in *S. aureus* for the catalytic site variant (13), suggesting that an enzyme/substrate intermediate is required to position the enzyme for efficient processing. However, it should also be noted that the protein processing step does not serve as an enzyme activation step; to the contrary, based on experiments performed in *S. aureus* it has been proposed that the LtaS cleavage step serves as a mechanism to inactivate the enzyme (16).

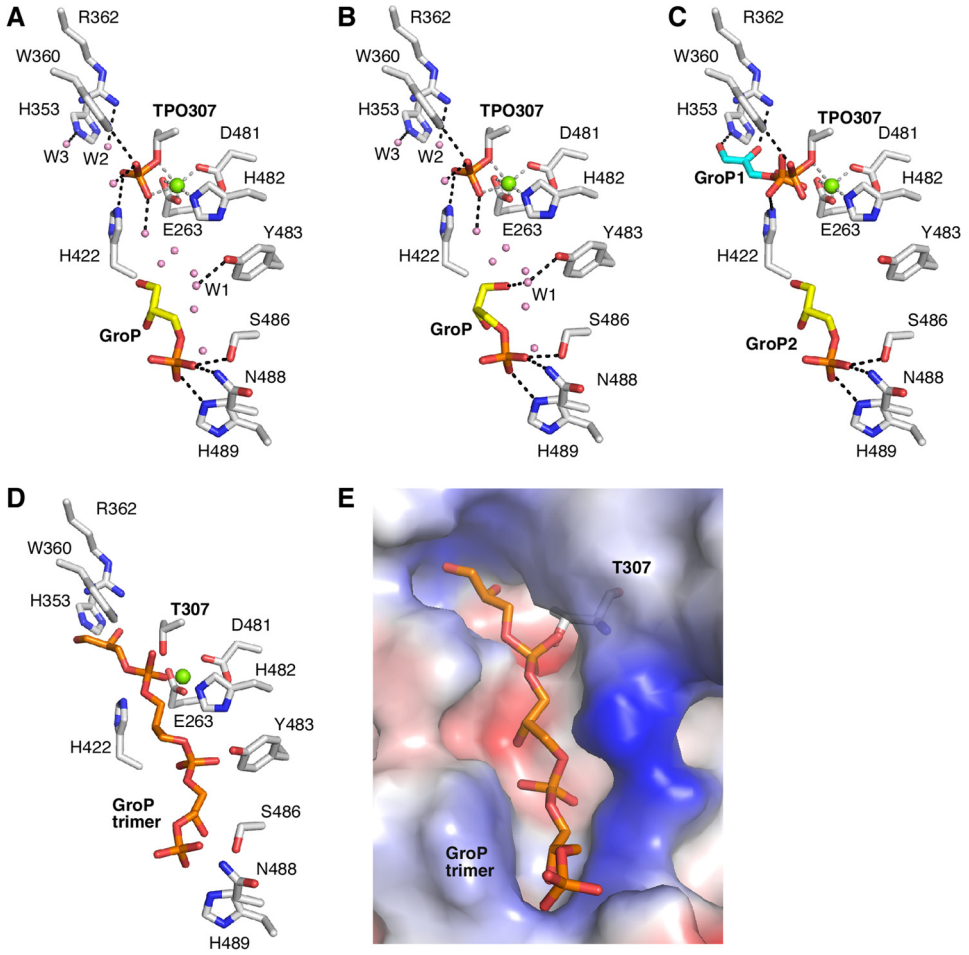

FIGURE 6. **Detailed view of the active center with metal and ligand interactions.** *A,* structural details of the eLtaS$_{Lm}$ active site showing the phospho-Thr intermediate (*TPO307*) and the metal binding site (as seen in chains A, E, and G). Hydrogen bonds are indicated as *gray lines* for the metal binding site and as *black lines* for the ligands. The water molecules that are conserved in all 11 monomers are represented as *spheres* in *pink*. Residues His-353, Arg-362, Trp-360, His-422, and two water molecules are involved in the binding of the phosphate group and phospho-Thr-307, Glu-263, Asp-481, and His-482 coordinate the Mg^{2+} ion. The GroP molecule, which is 6.5 Å removed from the catalytic residue, forms hydrogen bonds with Ser-486, Asn-488, and His-489. *B,* structural details of the eLtaS$_{Lm}$ active site showing the phospho-Thr intermediate (*TPO307*) and the metal binding site (as observed in chains B, C, D, F, H, I, J, and K). The GroP molecule forms hydrogen bonds with Ser-486, Asn-488, and His-489 like in *panel A* but in addition it also binds to a water molecule (*W1*), which in turn forms a hydrogen bond with Tyr-483. *C,* superposition between the catalytic site of eLtaS$_{Lm}$ and the GroP molecules trapped in the eLtaS$_{Sa}$-T300A structure (PDB code 2W5R). *D,* model of the eLtaS$_{Lm}$ active site bound to a GroP trimer. The GroP timer was produced and minimized with JLIGAND and superposed in PYMOL on the experimental crystal structure of the GroP-eLtaS$_{Lm}$ co-crystal structure. *E,* electrostatic potential representation of the eLtaSLm active site with the modeled GroP trimer. For clarity, the image is rotated by +30° around the *y* axis compared with *panel D*.

As expected, LTA production was restored to wild-type levels in the positive control strain 10403SΔ*ltaS* pPL3-*ltaS*$_{His6}$, whereas no LTA-specific signal was detected when extracts from the negative control strains were analyzed by Western blot using a polyglycerolphosphate-specific monoclonal LTA antibody (Fig. 7*A*). Expression of the S486A/N488A/H489A variant (LtaS$_{AAA}$) did not restore LTA production, revealing an essential function of the second GroP binding site for LTA production. Analysis of the single amino acid variants showed that residues Ser-486 and His-489, but not Asn-488 are important for the LTA polymerization step (Fig. 7*A*).

For successful LTA production, PG substrate hydrolysis and the GroP transfer reaction must take place. To determine whether the second GroP binding site is required specifically for PG hydrolysis, the WT and different eLtaS variants were produced in *E. coli*, purified, and used for *in vitro* enzyme reactions with fluorescently labeled NBD-PG lipid as substrate. As expected, mutating the catalytic Thr-307 residue abolished enzyme activity (Fig. 7*B*). The S486A and N488A variants retained the ability to hydrolyze PG, but the activity dropped by ~50% compared with wild-type eLtaS$_{Lm}$. The H489A and S486A/N488A/H489A (AAA) variants showed a marked decrease in activity to around 20% of WT (Fig. 7*B*). These data show that the second GroP binding site, in particular residue His-489, is also important for the PG hydrolysis step. The S486A variant, however, is of particular interest as this variant retains significant PG hydrolysis activity, whereas the PGP polymerase activity is nearly abolished. We would suggest that this is due to the inability of this variant to interact with the growing PGP chain and therefore, similar to what is observed naturally in the LTA primase enzyme, the two reactions are decoupled in this variant.

In a previous study, it has been shown that strain 10403SΔ*ltaS* has growth and morphological defects when propagated at 37 °C (3). To investigate if expression of any of the LtaS variants allows for sufficient LTA production to

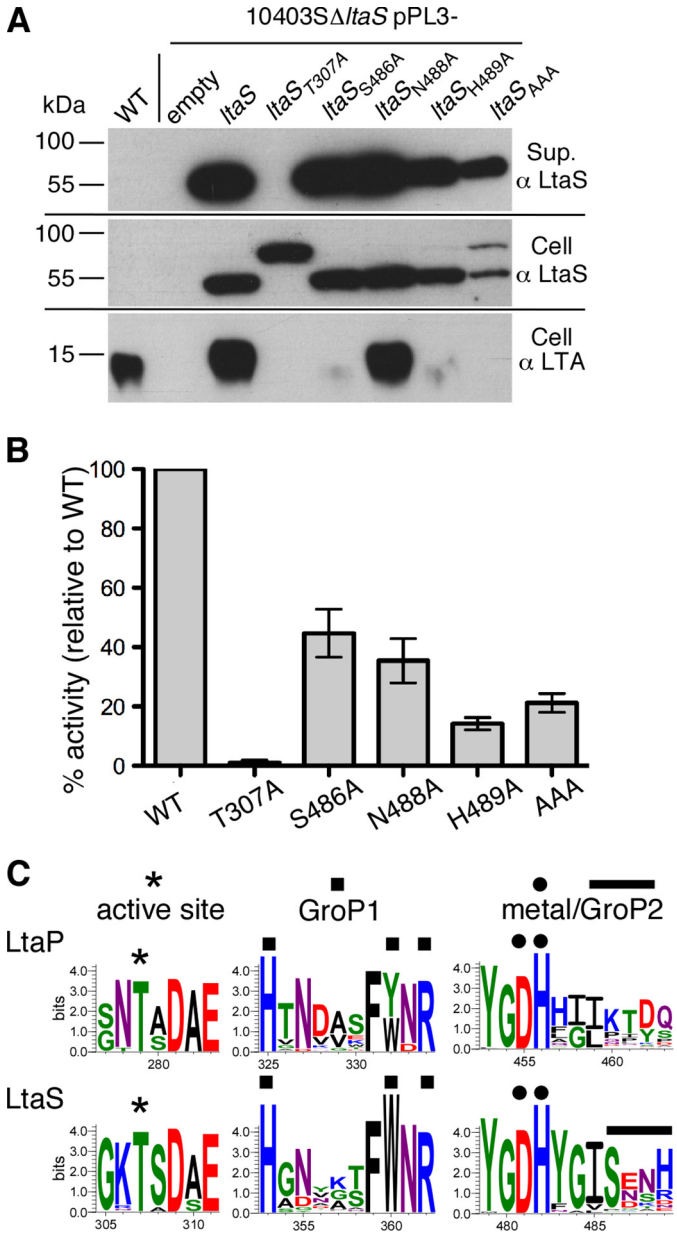

FIGURE 7. ***In vivo* and *in vitro* activity of eLtaS$_{Lm}$ GroP binding site variants and bioinformatics analysis of conserved binding residues.** *A*, detection of LtaS$_{Lm}$ protein and LTA by Western blot. Samples of wild-type *L. monocytogenes* 10403S (*WT*) and the 10403SΔ*ltaS*-derived strains containing an empty pPL3 vector or expressing the indicated LtaS$_{Lm}$ variants as C-terminal His tag fusion proteins were prepared for Western blot analysis. The LtaS protein was detected in the supernatant and cell wall-associated fractions using a His tag-specific antibody and LTA in the cell wall-associated fraction using a polyglycerolphosphate-specific antibody. *B*, *in vitro* enzyme activity assay with purified WT eLtaS$_{Lm}$ and the different eLtaS variants. Enzyme reactions were set up using the fluorescently labeled lipid NBD-PG as substrate. The reaction products were separated on TLC plates and the NBD-DAG product was quantified. Four independent experiments were performed and the enzyme activity of the eLtaS$_{Lm}$ protein (labeled WT in the graph) was set to 100% in each experiment. The relative activity of the different variants compared with WT eLtaS$_{Lm}$ was calculated and the average value and S.D. plotted. *C*, sequence logo motif of active site, metal binding, active site GroP (GroP1) and second GroP (GroP2) binding site residues. The 51 LtaP-like sequences (*top panels*) and the 1039 LtaS-type sequences (*bottom panels*) were aligned and logo motifs for selected amino acid regions are shown. Active site residue (*), GroP1 (■), GroP2 (−), and metal binding residues (●) are indicated and amino acid numbering for the respective *L. monocytogenes* protein is shown.

restore these defects, growth and microscopy analysis was performed with the complementation strains. As expected the *ltaS* deletion strain displayed the expected growth defect and a filamentation phenotype, which could be complemented by introducing a wild-type *ltaS* allele (Fig. 8). For the other complementation strains, only expression of the *ltaS*$_{T307A}$ allele did not restore the growth (Fig. 8*A*) and morphological defects (Fig. 8*B*). These results suggest that even if no signal for LTA is detected by Western blot, limited LTA synthesis must take place in these strains, which is sufficient to support normal growth and cell division.

Bioinformatics Analysis and Structure Guided Identification of LtaP and LtaS Enzyme Family Motifs—To obtain an overview of the distribution of LtaP and LtaS-type enzymes among Gram-positive bacteria and to investigate the conservation of the structural features identified in this study, bioinformatics analyses were performed. To this end, homologues to full-length LtaS and LtaP sequences were retrieved and filtered to those with an alignment length of more than 400 residues yielding 1088 sequences. This was done to remove proteins that do not contain an N-terminal membrane domain and are therefore unlikely involved in LTA production. Of the 1088 retrieved sequences, only 50 showed greater homology to LtaP than to LtaS (supplemental Table S1). Primase family enzymes are present in the different *Listeria* species and similar to *L. monocytogenes* these species also contain an LtaS-type enzyme. This analysis highlighted that a two-enzyme LTA synthesis system with highly divergent enzymes as seen in *Listeria* sp. is not widely distributed among bacteria (Fig. 9 and supplemental Table S1). For instance, *Bacillus* sp. also contain multiple enzymes, but they are more closely related to one another than to the two enzymes found in *Listeria* sp (Fig. 9 and supplemental Table S1). This could indicate that either a gene duplication event took place more recently in *Bacillus* sp. or that the divergent primase-like enzyme was only retained in a few species such as *Listeria, Thermotoga*, and *Paenibacillus* sp. Primase-like enzymes also appear to be present in a few specific bacterial strains such as *Planococcus donghaensis* MPA1U2, *Brevibacillus laterosporus* LMG, and *B. cereus cytotoxis* NVH 391–98 (Fig. 9 and supplemental Table S1). The latter strain was isolated from a fatal case of enteritis. It is therefore plausible that the gene coding for the primase enzyme was acquired through horizontal gene transfer from a *Listeria* strain by co-inhabiting the same ecological niche. It is also of note that the *Thermotoga* sp., *B. laterosporus* LMG, and several of the *Paenibacillus* sp. do not contain an LtaS-type enzyme and hence are unlikely to produce an actual LTA polymer.

As shown above, we have identified a second GroP binding site in LtaS$_{Lm}$ and confirmed its importance for LTA production experimentally. Next, we analyzed distribution of binding site residues Ser-486, Asn-488, and His-489 across LTA synthesis enzymes. Separate alignments were produced for the 1038 LtaS-type sequences and the 50 LtaP-type sequences. Subsequently, a logo motif was created to visualize the conservation of amino acids across the whole enzyme family (data not shown). As expected, the active site threonine, as well as the metal binding residues, were highly conserved and present in both LtaP and LtaS-type enzymes (Fig. 7*C*). In addition, con-

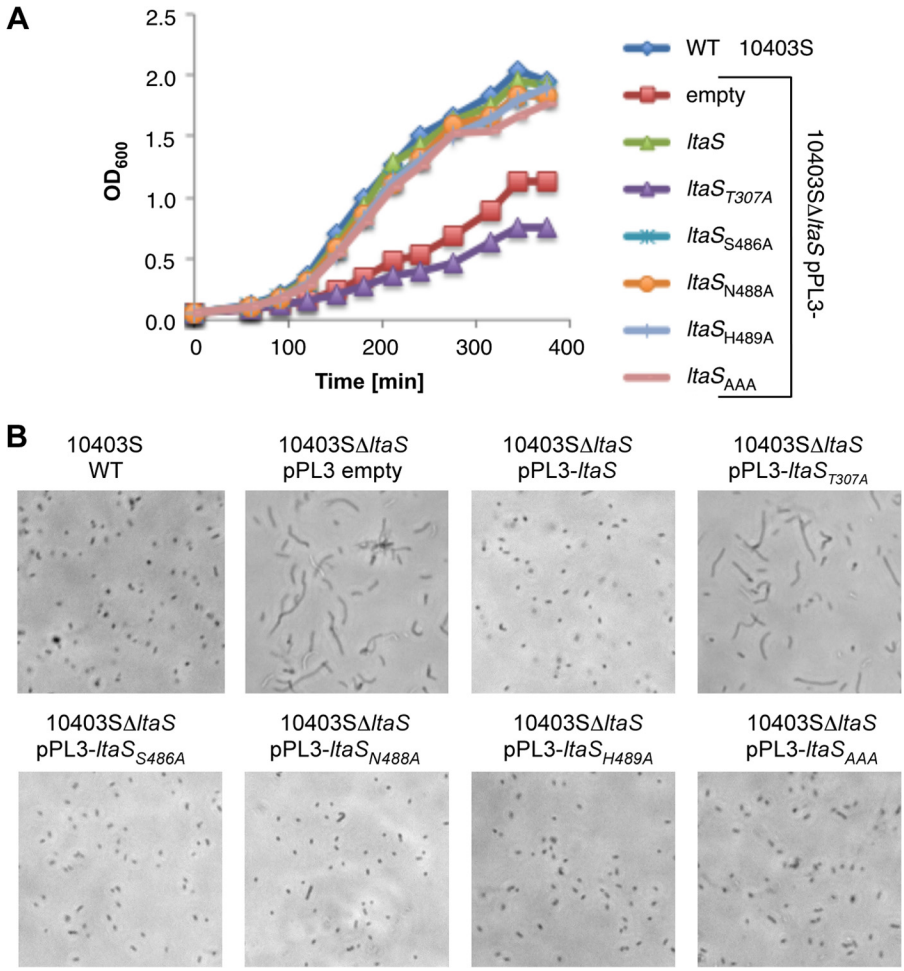

FIGURE 8. **Growth and microscopy analysis of wild-type *L. monocytogenes*, mutant, and complementation strains.** *A,* growth curves. The wild-type *L. monocytogenes* strain 10403S (WT) and 10403SΔ*ltaS*-derived strains containing an empty pPL3 vector or a pPL3 vector with the indicated *ltaS* allele were grown at 37 °C in BHI medium, A_{600} readings determined at timed intervals and plotted. *B*, microscopy analysis. The same strains as used for growth curves in *panel A* were analyzed by phase-contrast microscopy following growth at 37 °C.

served residues in the active site, which are required for binding of the GroP molecule within the active center, could also be identified in both enzyme types (Fig. 7*C*). The second GroP binding site residues corresponding to Ser-486 and His-488 in $LtaS_{Lm}$ were also conserved, however, only found in LtaS-type but not in primase-like enzymes (Fig. 7*C*). Based on our functional data, which showed that residues Ser-486 and His-488 are required for LTA production, we suggest that the absence of these residues is an important factor contributing to the inability of the LtaP enzyme to produce a PGP polymer.

DISCUSSION

Model for the Enzyme Reaction Mechanism and LTA Chain Extension of LtaS-type Enzymes—Our new data presented in this study combined with previous results allow us to speculate how the LTA synthesis proceeds. We suggest that the reaction is initiated by nucleophilic attack of Thr-307 to PG resulting in the breakage of the phosphoester bond yielding one molecule of DAG and a covalent GroP-Thr intermediate (Fig. 10). LtaS belongs to the alkaline phosphatase superfamily and arylsulfatase family, in which Ser and Thr residues are often phosphorylated to be activated (39). For this reason it has been postulated that phosphorylation of the catalytic Thr as observed in the *B. subtilis* LtaS structure is required for initiation of the reaction (13, 18). However, we show in the current study that this is not the case for $eLtaS_{Lm}$. Although the active site threonine residue is phosphorylated in the $eLtaS_{Lm}$ structure (Fig. 1), mass spectrometry analysis showed that this phosphorylation is likely an artifact caused by the purification of the protein from *E. coli* extracts as only a very small fraction of the protein obtained from the natural host *L. monocygenes* is phosphorylated (Fig. 3). The threonine phosphorylation is more likely to mimic the covalent GroP-Thr intermediate.

Next, the covalent GroP-Thr intermediate (GroP donor molecule) has to be attached to the incoming LTA chain (GroP acceptor molecule). In this study, we identified a second GroP binding site in the *L. monocytogenes* LtaS enzyme, which consists of residues S486A, N488A, and H489A. A reanalysis of the previously published *S. aureus* and *B. subtilis* eLtaS revealed that this binding site is identical in all three enzymes. It can be speculated that the tip of the LTA chain is bound in a similar manner to the GroP molecule within this second binding site. However, for a transfer reaction to occur, the enzyme would need to undergo a significant conformational change in order

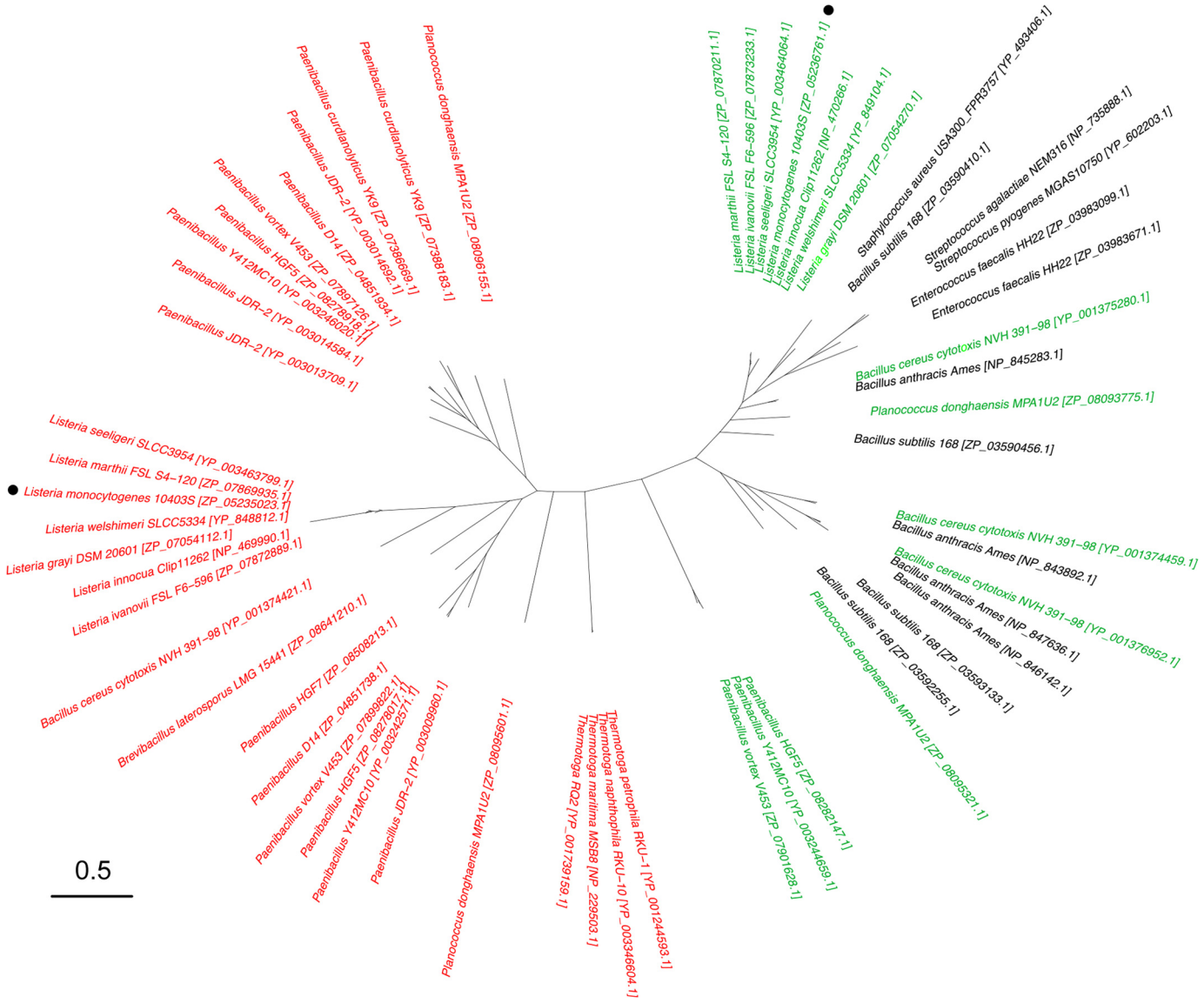

FIGURE 9. **Unrooted phylogenetic tree of representative LtaS and LtaP-type enzymes.** 1088 LtaS and LtaP sequence homologues were retrieved as described under "Experimental Procedures." An unrooted phylogenetic tree was generated for representative LtaS and LtaP-type enzymes. Thirty of 50 LtaP-like protein sequences are shown in *red* and 28 of the remaining 1038 LtaS-like sequences are shown in *green* if the same bacterial stain also contains an LtaP-like enzyme or in *black* if the bacterial strain only contains LtaS-like enzymes. For clarity, the majority of the LtaS-type sequences, which would fall onto the right side of the tree, are not shown. The *L. monocytogenes* 10403S proteins analyzed in this study are indicated with *dots*. The *scale bar* indicates the branch length unit of the tree as inferred using the program PROML and is the expected fraction of amino acids changed. A complete list of the organisms and RefSeq accession numbers can be found in supplemental Table S1 using the same color-coding with primase-like sequences shown in *red* and synthase-like sequences shown in *green* or *black*.

for the terminal hydroxyl group to reach the 6.3 Å removed charged active site threonine. Therefore we hypothesize that the trapped GroP molecule represents more likely the penultimate GroP subunit of a growing LTA chain (Figs. 6 and 10). Residues Lys-306 and Tyr-483 were located close to the active center, and could assist the binding of a terminal GroP subunit of an incoming chain by coordinating its phosphate group (Fig. 6). No electron density is observed for the side chain of Lys-306 in both the *Listeria* and *Staphylococcus* eLtaS enzymes, suggesting that the lysine is flexible and therefore could be used for stabilizing the phosphate group of an incoming terminal GroP (Fig. 6). It is of note that both Lys-306 and Tyr-483 are conserved residues among LtaS-type enzymes. In LtaP-type enzymes, where there is no requirement for binding of incoming GroP chains, these residues are replaced with Asn-278 and a range of amino acids at position 457 (Figs. 7*C*).

For the polymerization reaction to occur the proton of the terminal hydroxyl group of the incoming LTA chain must be displaced. No obvious candidate residues can be identified in the vicinity of this terminal GroP or near the bound GroP2. Previous findings showing that the full-length enzyme is required *in vivo* for LTA production highlights a crucial function of the membrane domain for enzyme function (17). One hypothesis is that a residue(s) within the transmembrane domain of the full-length LtaS enzyme could act as a base to remove a proton from the hydroxyl group of the acceptor GroP chain. Based on topology predictions, $LtaS_{Lm}$ has five transmembrane helices and two extracellular loops, which span res-

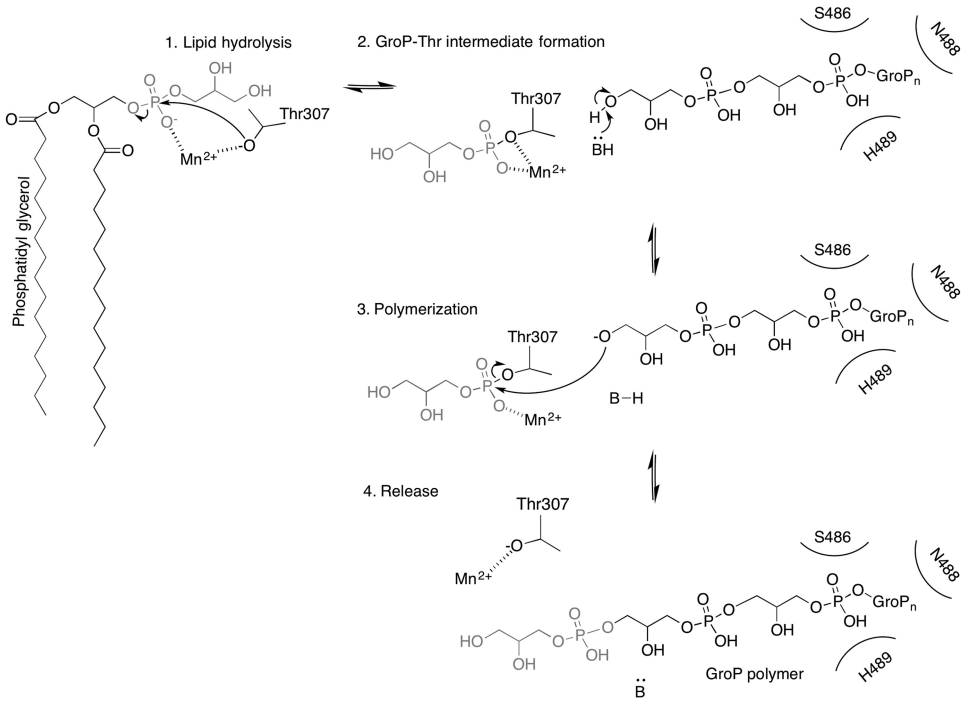

FIGURE 10. **Proposed reaction mechanism of LtaS$_{Lm}$.** The active site threonine is polarized by the Mn^{2+} ion allowing for a nucleophilic attack of Thr-307 to PG (*1*) generating the Thr-glycerolphosphate intermediate with the elimination of a DAG molecule (2). In our model the penultimate GroP molecule of the incoming GroP chain (GroP$_n$) would be held in place within the second GroP binding site. The hydroxyl group of the terminal GroP unit will be deprotonated by a base (amino acid residue or water) (*2*) allowing for a nucleophilic attack on the Thr-GroP intermediate to occur (*3*). The product of the reaction, the LTA chain extended by one GroP unit, is released and the cycle completed through the deprotonation of the base of the reaction and the catalytic Thr-307 is repolarized by the metal ion (*4*).

idues 35 to 48 (extracellular loop 1) and residues 98 to 105 (extracellular loop 2). Strikingly Asp-101 and Phe-102 within the second loop are highly conserved among LtaS-type enzymes but not in LtaP (data not shown) suggesting a possible functional role for these residues; in particular Asp-101 could act as a base required for the polymerization reaction. Once the terminal hydroxyl group is deprotonated it can act as a nucleophile to attack the phosphoester of the bound GroP-Thr assisted by the bound metal (Fig. 10).

To date, no structural information is available for the membrane portion of any of the LTA synthesis enzymes. Previously it has been reported that hybrid proteins, in which the membrane and extracellular domains of two functional proteins are swapped, are non-functional suggesting a specific interaction between the transmembrane and extracellular enzymatic domains (17). If a direct interaction between the two domains is crucial for enzyme function, one might expect interacting amino acids to co-vary within the two domains of LtaS enzymes. To explore this, a new larger alignment was made using 6943 sequences from the non-redundant database. Residue contacts were predicted using PSICOV and plotted alongside experimentally confirmed contacting amino acids based on the eLtaS$_{Lm}$ structure (Fig. 11). Using this analysis, several residues within the transmembrane region were predicted to be in contact with amino acid residues within the extracellular domain (primarily located in proximity of the active site or at the back of the molecule), supporting the notion of a physical interaction between the transmembrane and extracellular domain.

The LtaP$_{Lm}$ and LtaS$_{Lm}$ structures determined as part of this study provide information on the molecular basis for the restricted enzyme activity and inability of the LtaP$_{Lm}$ enzyme to polymerize LTA chains. Specifically, our work revealed that LtaP$_{Lm}$ has a smaller active site cavity, lacks a second GroP binding site, and that two conserved loop insertions results in subtle alterations to surface cavities. These data allowed us to propose a model on how the incoming LTA chain could bind during the chain extension step. Supported by bioinformatics analyses, we further suggest that a crucial catalytic residue for activating the GroP acceptor chain might be located within the transmembrane domain. To confirm this and to understand the functional significance of highly conserved amino acids within the extracellular loops or the conserved aspartic acid residues with the fourth transmembrane helix will require further studies and in particular a structural investigation on the full-length enzyme.

LTA synthesis enzymes are currently being actively pursued as target proteins for the development of novel antibiotics and recently, the first LtaS enzyme inhibitor was identified (4). Based on our findings, we would suggest that future structure-based design of LTA synthesis enzyme inhibitors should be extended to include the second GroP binding site. We envisage that targeting this binding site may offer a better chance of obtaining LtaS-specific inhibitors and decrease the possibility of obtaining compounds that are cross-reactive toward members of the same protein family such as mammalian alkaline phosphatases. Expanding the chemical landscape search to a larger enzyme area might increase the chances of

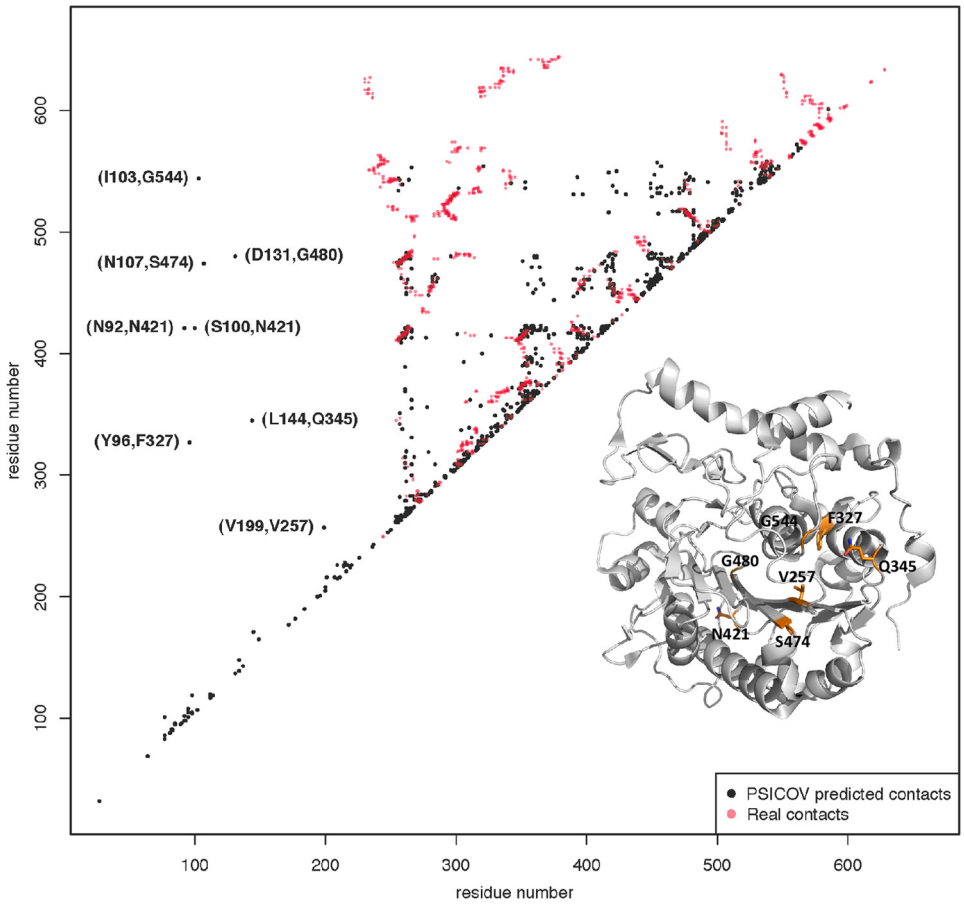

FIGURE 11. **Experimental and PSICOV-predicted contacts in $LtaS_{Lm}$.** PSICOV-predicted residue contacts using 6943 sequences are shown in *black* and experimentally confirmed contacting amino acids (Cβ-Cβ distance $<$8 Å) based on the $LtaS_{Lm}$ structure within the extracellular domain are shown in *red*. The eight predicted transmembrane domain extracellular domain contacts are labeled based on the $LtaS_{Lm}$ amino acid numbering. *Inset* shows e$LtaS_{Lm}$ structure with contacting amino acids in the extracellular domain highlighted in *orange*.

discovering new enzyme-specific inhibitors, which could be used to treat infections caused by important Gram-positive human pathogens.

Acknowledgments—We acknowledge the staff at beamline PROXIMA1 (SOLEIL synchrotron, Paris, France) and at beamlines I24 and I04-1 (DIAMOND synchrotron, Dicot, Oxford, United Kingdom) for assistance during data collection. We also thank Dr. Andrey Lebedev (STFC Rutherford Appleton Laboratory, Didcot, Oxford, UK) and Dr. Arwen Pearson (Hamburg Centre for Ultrafast Imaging, University of Hamburg, CFEL, Germany) for discussions about twinning and order-disorder structures.

REFERENCES

1. Gründling, A., and Schneewind, O. (2007) Synthesis of glycerol phosphate lipoteichoic acid in *Staphylococcus aureus*. *Proc. Natl. Acad. Sci. U.S.A.* **104,** 8478–8483
2. Oku, Y., Kurokawa, K., Matsuo, M., Yamada, S., Lee, B. L., and Sekimizu, K. (2009) Pleiotropic roles of polyglycerolphosphate synthase of lipoteichoic acid in growth of *Staphylococcus aureus* cells. *J. Bacteriol.* **191,** 141–151
3. Webb, A. J., Karatsa-Dodgson, M., and Gründling, A. (2009) Two-enzyme systems for glycolipid and polyglycerolphosphate lipoteichoic acid synthesis in *Listeria monocytogenes*. *Mol. Microbiol.* **74,** 299–314
4. Richter, S. G., Elli, D., Kim, H. K., Hendrickx, A. P., Sorg, J. A., Schneewind, O., and Missiakas, D. (2013) Small molecule inhibitor of lipoteichoic acid synthesis is an antibiotic for Gram-positive bacteria. *Proc. Natl. Acad. Sci. U.S.A.* **110,** 3531–3536
5. Fisher, W. (1990) *Bacterial Phosphoglycolipids and Lipoteichoic Acids*, Plenum Press, New York
6. Percy, M. G., and Gründling, A. (2014) Lipoteichoic acid synthesis and function in Gram-positive bacteria. *Annu. Rev. Microbiol.* **68,** 81–100
7. Hether, N. W., and Jackson, L. L. (1983) Lipoteichoic acid from *Listeria monocytogenes*. *J. Bacteriol.* **156,** 809–817
8. Uchikawa, K., Sekikawa, I., and Azuma, I. (1986) Structural studies on lipoteichoic acids from four *Listeria* strains. *J. Bacteriol.* **168,** 115–122
9. Koch, H. U., Haas, R., and Fischer, W. (1984) The role of lipoteichoic acid biosynthesis in membrane lipid metabolism of growing *Staphylococcus aureus*. *Eur. J. Biochem.* **138,** 357–363
10. Taron, D. J., Childs, W. C., 3rd, and Neuhaus, F. C. (1983) Biosynthesis of D-alanyl-lipoteichoic acid: role of diglyceride kinase in the synthesis of phosphatidylglycerol for chain elongation. *J. Bacteriol.* **154,** 1110–1116
11. Karatsa-Dodgson, M., Wörmann, M. E., and Gründling, A. (2010) *In vitro* analysis of the *Staphylococcus aureus* lipoteichoic acid synthase enzyme using fluorescently labeled lipids. *J. Bacteriol.* **192,** 5341–5349
12. Reichmann, N. T., and Gründling, A. (2011) Location, synthesis and function of glycolipids and polyglycerolphosphate lipoteichoic acid in Gram-positive bacteria of the phylum Firmicutes. *FEMS Microbiol. Lett.* **319,** 97–105
13. Lu, D., Wörmann, M. E., Zhang, X., Schneewind, O., Gründling, A., and Freemont, P. S. (2009) Structure-based mechanism of lipoteichoic acid synthesis by *Staphylococcus aureus* LtaS. *Proc. Natl. Acad. Sci. U.S.A.* **106,** 1584–1589
14. Powers, M. E., Smith, P. A., Roberts, T. C., Fowler, B. J., King, C. C., Trauger, S. A., Siuzdak, G., and Romesberg, F. E. (2011) Type I signal peptidase and protein secretion in *Staphylococcus epidermidis*. *J. Bacte-*

riol. **193,** 340–348
15. Antelmann, H., Williams, R. C., Miethke, M., Wipat, A., Albrecht, D., Harwood, C. R., and Hecker, M. (2005) The extracellular and cytoplasmic proteomes of the non-virulent *Bacillus anthracis* strain UM23C1–2. *Proteomics* **5,** 3684–3695
16. Wörmann, M. E., Reichmann, N. T., Malone, C. L., Horswill, A. R., and Gründling, A. (2011) Proteolytic cleavage inactivates the *Staphylococcus aureus* lipoteichoic acid synthase. *J. Bacteriol.* **193,** 5279–5291
17. Wörmann, M. E., Corrigan, R. M., Simpson, P. J., Matthews, S. J., and Gründling, A. (2011) Enzymatic activities and functional interdependencies of *Bacillus subtilis* lipoteichoic acid synthesis enzymes. *Mol. Microbiol.* **79,** 566–583
18. Schirner, K., Marles-Wright, J., Lewis, R. J., and Errington, J. (2009) Distinct and essential morphogenic functions for wall- and lipo-teichoic acids in *Bacillus subtilis*. *EMBO J.* **28,** 830–842
19. Lauer, P., Chow, M. Y., Loessner, M. J., Portnoy, D. A., and Calendar, R. (2002) Construction, characterization, and use of two *Listeria monocytogenes* site-specific phage integration vectors. *J. Bacteriol.* **184,** 4177–4186
20. Walter, T. S., Meier, C., Assenberg, R., Au, K. F., Ren, J., Verma, A., Nettleship, J. E., Owens, R. J., Stuart, D. I., and Grimes, J. M. (2006) Lysine methylation as a routine rescue strategy for protein crystallization. *Structure* **14,** 1617–1622
21. Kabsch, W. (2010) Xds. *Acta Crystallogr. D Biol. Crystallogr.* **66,** 125–132
22. Evans, P. (2006) Scaling and assessment of data quality. *Acta Crystallogr. D Biol. Crystallogr.* **62,** 72–82
23. Winn, M. D., Ballard, C. C., Cowtan, K. D., Dodson, E. J., Emsley, P., Evans, P. R., Keegan, R. M., Krissinel, E. B., Leslie, A. G., McCoy, A., McNicholas, S. J., Murshudov, G. N., Pannu, N. S., Potterton, E. A., Powell, H. R., Read, R. J., Vagin, A., and Wilson, K. S. (2011) Overview of the CCP4 suite and current developments. *Acta Crystallogr. D Biol. Crystallogr.* **67,** 235–242
24. Adams, P. D., Afonine, P. V., Bunkóczi, G., Chen, V. B., Davis, I. W., Echols, N., Headd, J. J., Hung, L. W., Kapral, G. J., Grosse-Kunstleve, R. W., McCoy, A. J., Moriarty, N. W., Oeffner, R., Read, R. J., Richardson, D. C., Richardson, J. S., Terwilliger, T. C., and Zwart, P. H. (2010) PHENIX: a comprehensive Python-based system for macromolecular structure solution. *Acta Crystallogr. D Biol. Crystallogr.* **66,** 213–221
25. Emsley, P., Lohkamp, B., Scott, W. G., and Cowtan, K. (2010) Features and development of COOT. *Acta Crystallogr. D Biol. Crystallogr.* **66,** 486–501
26. Murshudov, G. N., Skubák, P., Lebedev, A. A., Pannu, N. S., Steiner, R. A., Nicholls, R. A., Winn, M. D., Long, F., and Vagin, A. A. (2011) REFMAC5 for the refinement of macromolecular crystal structures. *Acta Crystallogr. D Biol. Crystallogr.* **67,** 355–367
27. Davis, I. W., Leaver-Fay, A., Chen, V. B., Block, J. N., Kapral, G. J., Wang, X., Murray, L. W., Arendall, W. B., 3rd, Snoeyink, J., Richardson, J. S., and Richardson, D. C. (2007) MolProbity: all-atom contacts and structure validation for proteins and nucleic acids. *Nucleic Acids Res.* **35,** W375–W383
28. Bergfors, T. (2003) Seeds to crystals. *J. Struct. Biol.* **142,** 66–76
29. Long, F., Vagin, A. A., Young, P., and Murshudov, G. N. (2008) BALBES: a molecular-replacement pipeline. *Acta Crystallogr. D Biol. Crystallogr.* **64,** 125–132
30. Lebedev, A. A., Young, P., Isupov, M. N., Moroz, O. V., Vagin, A. A., and Murshudov, G. N. (2012) JLigand: a graphical tool for the CCP4 template-restraint library. *Acta Crystallogr. D Biol. Crystallogr.* **68,** 431–440
31. Pruitt, K. D., Tatusova, T., Klimke, W., and Maglott, D. R. (2009) NCBI Reference Sequences: current status, policy and new initiatives. *Nucleic Acids Res.* **37,** D32–D36
32. Altschul, S. F., Madden, T. L., Schäffer, A. A., Zhang, J., Zhang, Z., Miller, W., and Lipman, D. J. (1997) Gapped BLAST and PSI-BLAST: a new generation of protein database search programs. *Nucleic Acids Res.* **25,** 3389–3402
33. Edgar, R. C. (2004) MUSCLE: multiple sequence alignment with high accuracy and high throughput. *Nucleic Acids Res.* **32,** 1792–1797
34. Felsenstein, J. (1989) PHYLIP-Phylogeny interference package (version 3.2). *Cladistics* **5,** 164–166
35. Paradis, E., Claude, J., and Strimmer, K. (2004) APE: analyses of phylogenetics and evolution in R language. *Bioinformatics* **20,** 289–290
36. Crooks, G. E., Hon, G., Chandonia, J. M., and Brenner, S. E. (2004) WebLogo: a sequence logo generator. *Genome Res.* **14,** 1188–1190
37. Jones, D. T., Buchan, D. W., Cozzetto, D., and Pontil, M. (2012) PSICOV: precise structural contact prediction using sparse inverse covariance estimation on large multiple sequence alignments. *Bioinformatics* **28,** 184–190
38. Bond, C. S., Clements, P. R., Ashby, S. J., Collyer, C. A., Harrop, S. J., Hopwood, J. J., and M, J. G. (1997) Structure of a human lysosomal sulphatase. *Structure* **5,** 227–289
39. Krogh, A., Larsson, B., von Heijne, G., and Sonnhammer, E. L. (2001) Predicting transmembrane protein topology with a hidden Markov model: application to complete genomes. *J. Mol. Biol.* **305,** 567–580
40. Simon, R., Priefer, U., and Pühler, A. (1983) A broad host range mobilization system for *in vitro* genetic engineering: transposon mutagenesis in Gram negative bacteria. *Nat. Biotechnol.* **1,** 784–791
41. Gründling, A., Burrack, L. S., Bouwer, H. G., and Higgins, D. E. (2004) *Listeria monocytogenes* regulates flagellar motility gene expression through MogR, a transcriptional repressor required for virulence. *Proc. Natl. Acad. Sci. U.S.A.* **101,** 12318–12323
42. Bishop, D. K., and Hinrichs, D. J. (1987) Adoptive transfer of immunity to *Listeria monocytogenes. The influence of in vitro* stimulation on lymphocyte subset requirements. *J. Immunol.* **139,** 2005–2009
43. Karplus, P. A., and Diederichs, K. (2012) Linking crystallographic model and data quality. *Science* **336,** 1030–1033